

Lawrence Berkeley National Laboratory

Recent Work

Title

Germline Chd8 haploinsufficiency alters brain development in mouse.

Permalink

<https://escholarship.org/uc/item/0ck9n78k>

Journal

Nature neuroscience, 20(8)

ISSN

1097-6256

Authors

Gompers, Andrea L
Su-Feher, Linda
Ellegood, Jacob
et al.

Publication Date

2017-08-01

DOI

10.1038/nn.4592

Peer reviewed

Germline *Chd8* haploinsufficiency alters brain development in mouse

Andrea L Gompers^{1,2,10}, Linda Su-Feher^{1,2,10} , Jacob Ellegood^{3,10}, Nycole A Copping^{1,4,10}, M Asrafuzzaman Riyadh^{5,10}, Tyler W Stradleigh^{1,2}, Michael C Pride^{1,4}, Melanie D Schaffler^{1,4}, A Ayanna Wade^{1,2} , Rinaldo Catta-Preta^{1,2} , Iva Zdilar^{1,2}, Shreya Louis^{1,2} , Gaurav Kaushik⁵, Brandon J Mannion⁶, Ingrid Plajzer-Frick⁶, Veena Afzal⁶, Axel Visel⁶⁻⁸ , Len A Pennacchio^{6,7}, Diane E Dickel⁶, Jason P Lerch^{3,9}, Jacqueline N Crawley^{1,4}, Konstantinos S Zarbalis⁵, Jill L Silverman^{1,4} & Alex S Nord^{1,2} 

The chromatin remodeling gene *CHD8* represents a central node in neurodevelopmental gene networks implicated in autism. We examined the impact of germline heterozygous frameshift *Chd8* mutation on neurodevelopment in mice. *Chd8^{+del5}* mice displayed normal social interactions with no repetitive behaviors but exhibited cognitive impairment correlated with increased regional brain volume, validating that phenotypes of *Chd8^{+del5}* mice overlap pathology reported in humans with *CHD8* mutations. We applied network analysis to characterize neurodevelopmental gene expression, revealing widespread transcriptional changes in *Chd8^{+del5}* mice across pathways disrupted in neurodevelopmental disorders, including neurogenesis, synaptic processes and neuroimmune signaling. We identified a co-expression module with peak expression in early brain development featuring dysregulation of RNA processing, chromatin remodeling and cell-cycle genes enriched for promoter binding by *Chd8*, and we validated increased neuronal proliferation and developmental splicing perturbation in *Chd8^{+del5}* mice. This integrative analysis offers an initial picture of the consequences of *Chd8* haploinsufficiency for brain development.

DNA packaging determines the transcriptional potential of a cell and is central to the development and function of metazoan cell types¹. Chromatin remodeling complexes control the local chromatin state, yielding either transcriptional activation or repression. Pluripotency, proliferation and differentiation are dependent on genomic regulation at the chromatin level, and proteins that control chromatin packaging are critical in development and cancer². Although many chromatin remodeling factors function across organ systems, case-sequencing efforts have linked mutations of chromatin genes with specific, causal roles in neurodevelopmental disorders (NDDs)³⁻⁶. This finding is particularly strong for rare and *de novo* mutations in autism spectrum disorder (ASD)^{7,8}. Understanding how mutations to chromatin remodeling genes affect transcriptional regulation during brain development may reveal developmental and cellular mechanisms driving NDDs.

A key gene that has emerged from studies profiling rare and *de novo* coding variation in ASD is the gene *CHD8*, which encodes the chromatin remodeler CHD8 (chromodomain helicase DNA-binding protein 8)⁹. In addition to ASD, human individuals harboring *CHD8* mutations exhibit macrocephaly, distinct craniofacial morphology, mild-to-severe intellectual disability (ID) and gastrointestinal problems⁹. Homozygous deletion of *Chd8* in mice is lethal at early embryonic stages¹⁰. *Chd8* knockdown in zebrafish recapitulates

macrocephaly and gastrointestinal phenotypes^{9,11}, suggesting a high degree of evolutionary conservation of CHD8 function in development. It has been proposed that CHD8 achieves this regulatory function in brain development by binding to relevant gene promoters and enhancers¹¹⁻¹⁴. Although recent mouse studies indicate that *Chd8* is required in neurogenesis and that mutations to *Chd8* cause behavioral phenotypes^{13,15}, important questions remain regarding the role of *Chd8* in regulating neurodevelopment, brain structure and behavior via direct and indirect transcriptional regulation. Characterizing the functional impact of germline heterozygous *CHD8* mutation on brain development could reveal specific and generalizable mechanisms linking chromatin biology to NDD pathology. Toward this goal, we generated a germline 5-base-pair (bp) deletion in *Chd8* using CRISPR/Cas9 genome engineering and assayed neuroanatomic, behavioral and transcriptional phenotypes associated with *Chd8* haploinsufficiency in the developing mouse brain.

RESULTS

Mice harboring heterozygous germline *Chd8* mutation exhibit megalencephaly

We used CRISPR/Cas9 targeting of C57BL/6N oocytes to generate mice harboring 5-bp or 14-bp deletions in *Chd8* exon 5, upstream of

¹Department of Psychiatry and Behavioral Sciences, University of California, Davis, Davis, California, USA. ²Department of Neurobiology, Physiology and Behavior, University of California, Davis, Davis, California, USA. ³Mouse Imaging Centre, The Hospital for Sick Children, Toronto, Ontario, Canada. ⁴MIND Institute, School of Medicine, University of California, Davis, Davis, California, USA. ⁵Department of Pathology and Laboratory Medicine, Shriners Hospitals for Children, Institute for Pediatric Regenerative Medicine, University of California, Davis, Sacramento, California, USA. ⁶Lawrence Berkeley National Laboratory, Functional Genomics Department, Berkeley, California, USA. ⁷Department of Energy Joint Genome Institute, Walnut Creek, California, USA. ⁸School of Natural Sciences, University of California, Merced, California, USA. ⁹Department of Medical Biophysics, University of Toronto, Toronto, Ontario, Canada. ¹⁰These authors contributed equally to this work. Correspondence should be addressed to A.S.N. (asnord@ucdavis.edu).

Received 7 September 2016; accepted 23 May 2017; published online 26 June 2017; doi:10.1038/nn.4592

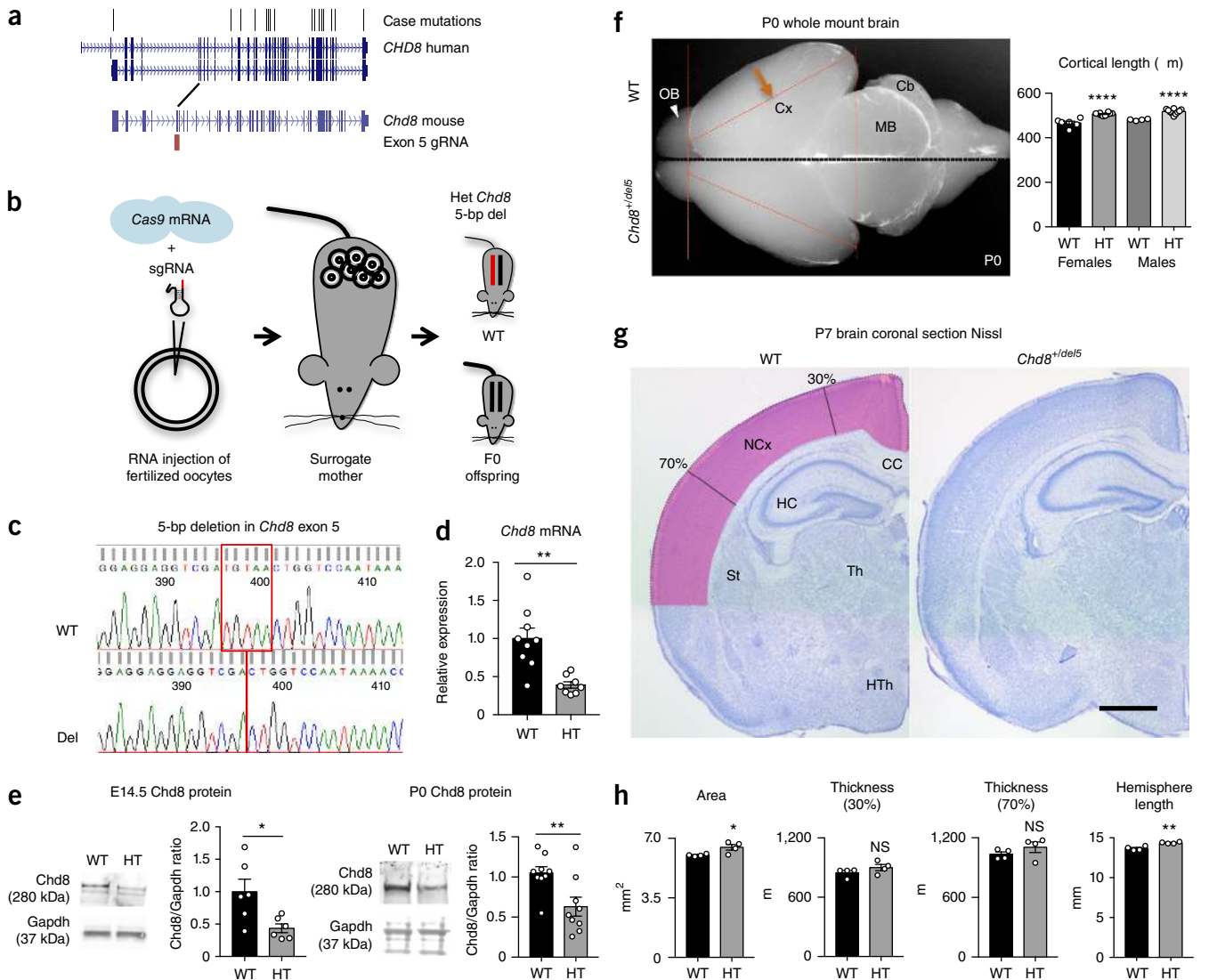


Figure 1 *Chd8*^{+del5} mouse model. (a) Location of case mutations in human *CHD8*⁹ (top) and corresponding guideRNA sequence homology for Cas9-targeting of mouse *Chd8* (bottom). (b) Schematic of mouse line generation. Het, heterozygous; del, deletion. (c) Sequence trace showing 5-bp deletion in exon 5. (d) qRT-PCR showing reduction of RNA in *Chd8*^{+del5} (HT) forebrain at P0 (***P* = 0.0076; *n* = 9 WT, 8 *Chd8*^{+del5}). (e) Western blot of *Chd8*^{+del5} mice, showing reduction of Chd8 protein in *Chd8*^{+del5} forebrain at E14.5 (**P* = 0.02; *n* = 6 WT, 6 *Chd8*^{+del5}) and P0 (***P* = 0.0089; *n* = 9 WT, 9 *Chd8*^{+del5}). (f) Whole-mount brain of *Chd8*^{+del5} mouse at P0 reveals increased cortical length (denoted by orange arrow and line), indicative of megalencephaly. OB, olfactory bulb; Cx, cortex; MB, midbrain; Cb, cerebellum. (*****P* < 0.0001; WT *n* = 4 male, 6 female; *Chd8*^{+del5} *n* = 10 male, 10 female). (g) Representative coronal sections of WT and *Chd8*^{+del5} brains at P7 visualized with Nissl stain. Scale bar, 1 mm. Pink shading, measured neocortical area; NCx, neocortex; St, striatum; CC, corpus callosum; HC, hippocampus; Th, thalamus; HTh, hypothalamus. (h) Plots of cortical area, thickness at 30% and 70% distance from the dorsal midline and cortical hemispheric circumference (dots represent individual samples; *n* = 4 mice each for both genotypes; area, **P* = 0.0328; thickness (30%) *P* = 0.224, thickness (70%) *P* = 0.268; length, ***P* = 0.0026). *P* values derived using Student's *t*-test for **d**, **e** and **h** and using one-way ANOVA for **f**. Error bars represent mean ± s.e.m.

the majority of identified human mutations⁹ (Fig. 1a–c). F0 mutation carrier lines were expanded via breeding to wild-type C57BL/6N (WT) mice. Heterozygous male mice were bred for at least four generations before further experiments, and multiple litters were used for all experiments to eliminate potential off-target mutations. Consistent with an earlier study¹⁰, the presumed *Chd8* frameshift alleles resulted in embryonic lethality in homozygous mutants, but heterozygous (*Chd8*^{+del5}) mice were viable, reached a normal lifespan and were fertile irrespective of sex.

We performed quantitative reverse-transcription PCR (qRT-PCR) and western blot analysis on brain lysates, using an N-terminus Chd8

antibody that has been used previously used for Chd8 chromatin immunoprecipitation followed by deep sequencing (ChIP-seq)¹². Heterozygous mutation resulted in decreased *Chd8* transcript and protein at embryonic day (E)14.5, postnatal day (P)0 and in adults (Fig. 1d,e and Supplementary Fig. 1a–c). We identified a band representing full-length Chd8 (~280 kDa), which was consistently significantly reduced in *Chd8*^{+del5} mice at all stages (Supplementary Fig. 1a–c). We also observed a smaller ~110 kDa band, similar in size to what has been reported as a short Chd8 isoform¹³, which displayed inconsistent trends of lower expression in *Chd8*^{+del5} mice (Supplementary Fig. 1a–c). We performed RNA sequencing on E12.5 WT mice and

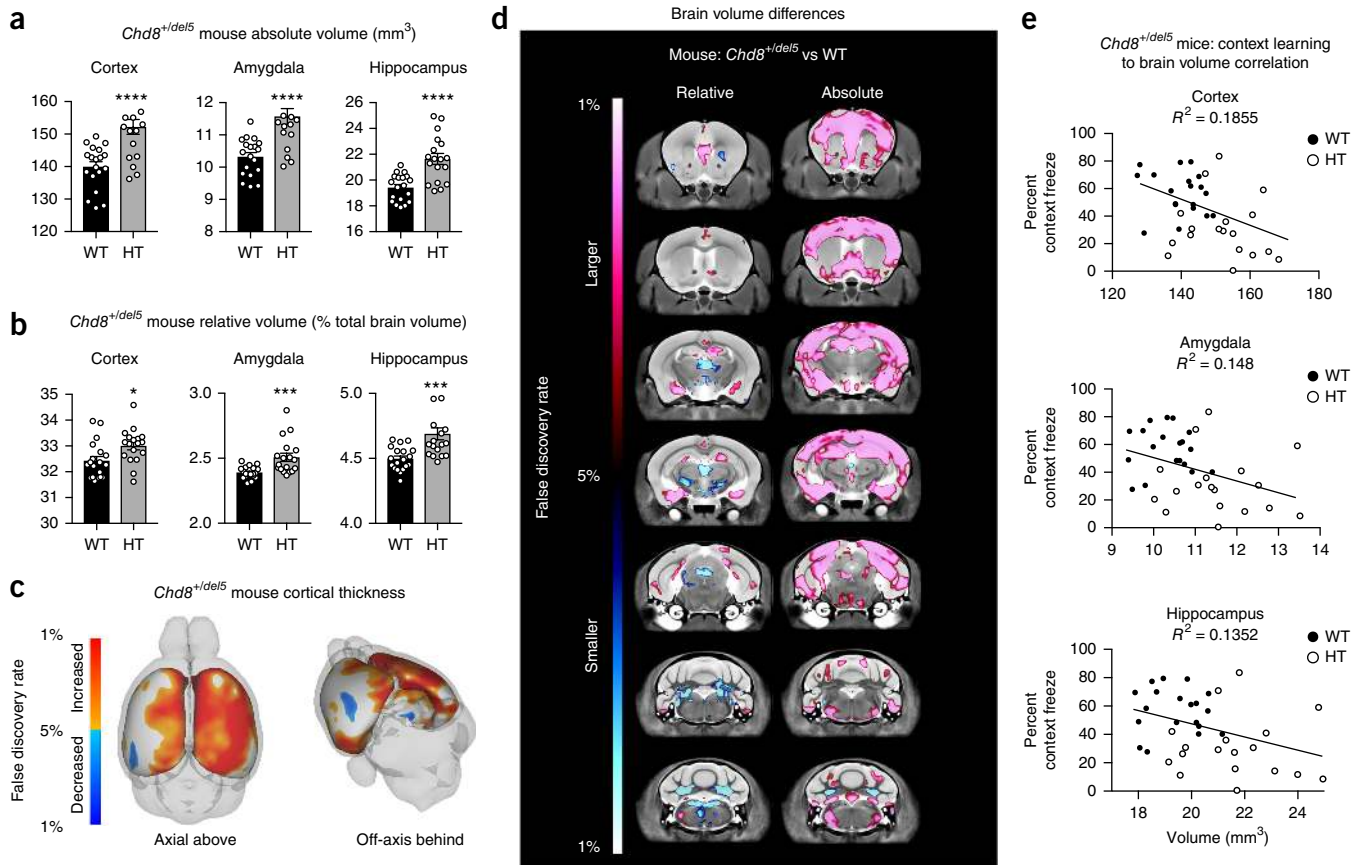


Figure 3 *Chd8* haploinsufficiency drives megalencephaly and cognitive impairment in mouse. (a) MRI revealed significant increases in absolute regional volume of cerebral cortex (**** $P < 0.0001$), amygdala (**** $P < 0.0001$) and hippocampus (**** $P < 0.0001$) in *Chd8*^{+/-del5} (HT) mice ($n = 19$ WT, 18 *Chd8*^{+/-del5}; see **Supplementary Table 1** for full regional statistical analysis and FDR values). (b) Increases in volume are still significant for the cortex (* $P = 0.00147$), amygdala (*** $P = 0.0010$) and hippocampus (*** $P = 0.0004$) after correction for absolute brain volume. (c) Increased cortical thickness is present in *Chd8*^{+/-del5} mice. (d) Voxel-wise differences in volume between *Chd8*^{+/-del5} and WT littermates. (e) Concordance of specific brain region size and cognitive impairment in *Chd8*^{+/-del5} mice (context conditioning score; R^2 : cortex = 0.1855, hippocampus = 0.148, amygdala = 0.1352). Student's *t*-test used for **a** and **b**; error bars in **a** and **b** represent mean \pm s.e.m.

(**Supplementary Fig. 2**), indicating that *Chd8*^{+/-del5} mice exhibited deficits in learning and memory.

Behaviors relevant to diagnostic symptoms of ASD were assessed using corroborative assays of social and repetitive behaviors¹⁷. Normal sociability was detected in both genotypes (**Fig. 2d–i**). Time spent in the chamber with the novel mouse was greater than with the novel object, meeting the definition of sociability in this assay, for both WT and *Chd8*^{+/-del5} mice (**Fig. 2d**; WT: $F_{1,19} = 16.31$, $P = 0.0007$; *Chd8*^{+/-del5}: $F_{1,18} = 9.744$, $P = 0.0059$). No sex differences were detected ($F_{1,37} = 2.16$, $P = 0.149$). Time spent sniffing the novel mouse was greater than time spent sniffing the novel object in both WT and *Chd8*^{+/-del5} (**Fig. 2e**; WT: $F_{1,18} = 7.00369$, $P = 0.0164$; *Chd8*^{+/-del5}: $F_{1,17} = 12.8051$, $P = 0.0023$), with no sex differences ($F_{1,35} = 0.0985$, $P = 0.7555$). The number of entries into the side chambers was not affected by genotype in the social phase (**Fig. 2f**; $F_{1,37} = 0.11$, $P = 0.73$) or in the habituation phase ($F_{1,37} = 0.30$, $P = 0.584$), indicating normal exploratory activity in both genotypes during the assay. No deficits were observed in social parameters in male *Chd8*^{+/-del5} mice during male–female reciprocal social interaction (**Fig. 2g–i**). WT and *Chd8*^{+/-del5} males spent similar amounts of time sniffing (**Fig. 2g**; $t_{1,17} = 0.9409$, $P = 0.3599$) and following (**Fig. 2h**; $t_{1,17} = 0.5785$, $P = 0.5705$) the estrous WT female. Ultrasonic vocalizations during male–female interaction showed no genotype difference in number of emitted calls

(**Fig. 2i**; $t_{1,17} = 0.1634$, $P = 0.8722$). No spontaneous stereotypies or repetitive behaviors were observed in the self-grooming assay (**Fig. 2j**; $t_{1,38} = 0.8552$, $P = 0.3978$) or numbers of marbles buried (**Fig. 2k**; $t_{1,38} = 1.0151$, $P = 0.3165$). No sex differences were detected (self-grooming: $t_{1,36} = -0.504$, $P = 0.619$; marble burying: $t_{1,38} = 1.4883$, $P = 0.1449$). Open-field locomotor activity did not differ between genotypes (**Fig. 2l**; $t_{1,38} = 1.1795$, $P = 0.2455$), indicating normal exploratory and motor abilities. No substantial differences were observed in body weight or other relevant measures of general health in adult *Chd8*^{+/-del5} mice.

Analysis of *Chd8*^{+/-del5} adult brain structure via MRI

Intact brains were collected from the same mice that comprised the first cohort of behavioral phenotyping. Structural MRI was performed to identify changes in absolute (mm³) and relative regional brain volume and connectivity. In regional analysis, cortex was most affected, with a 7.5% increase in absolute volume in *Chd8*^{+/-del5} mice (false discovery rate (FDR) = 1%). Similarly, cerebral white matter and cerebral gray matter were larger in *Chd8*^{+/-del5} mice at 5.4% (FDR = 3%) and 6.1% (FDR = 2%), respectively. We assessed 159 independent brain regions with divisions across the cortex, subcortical areas and cerebellum (full results reported in **Supplementary Table 1**). *Chd8*^{+/-del5} mice showed robust increases in absolute volume across cortical regions, hippocampus (+10.3%, FDR < 1%) and amygdala (+11.0%, FDR < 1%; **Fig. 3a**).

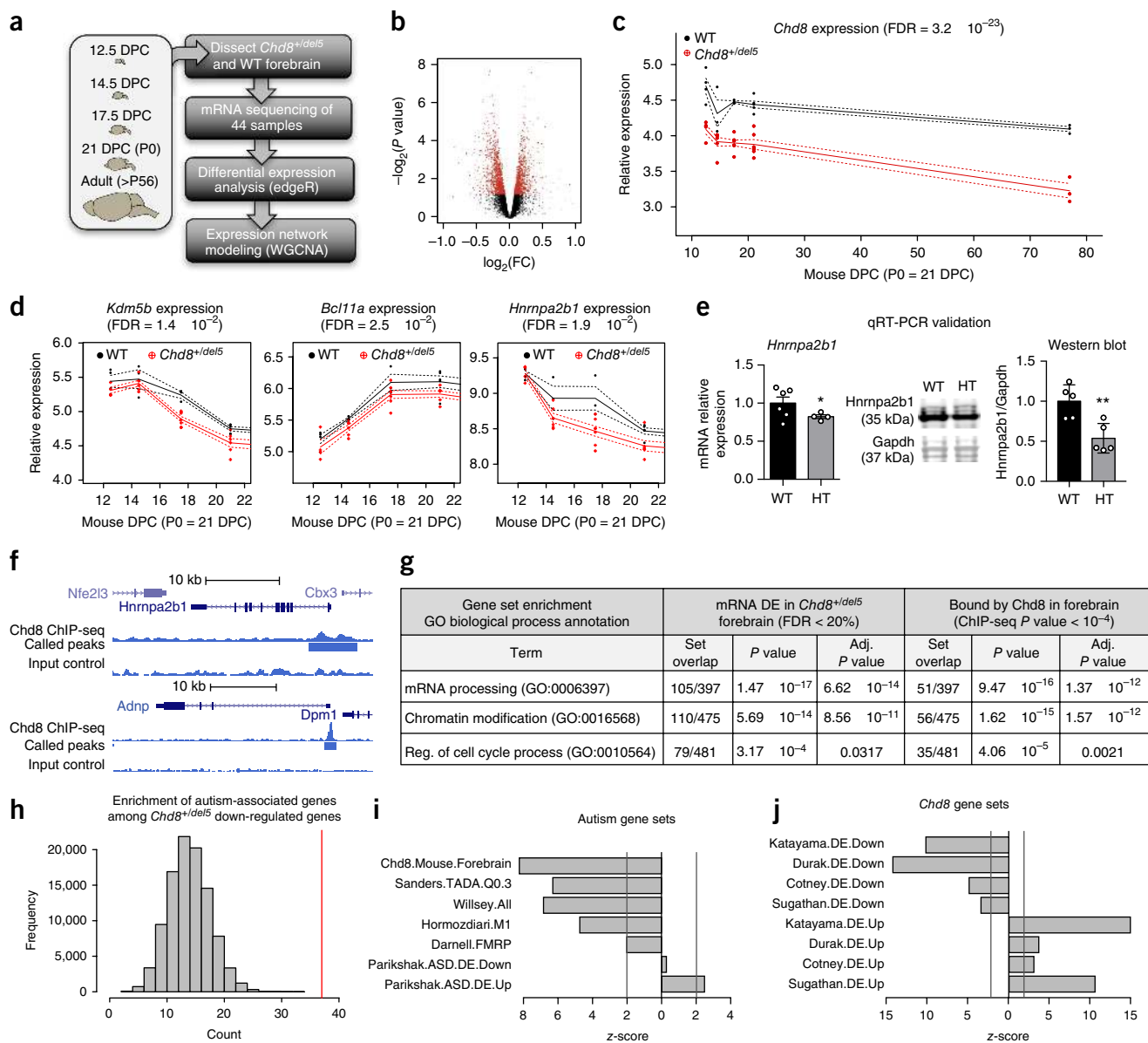


Figure 4 Differential gene expression in *Chd8*^{+/del5} neurodevelopment. **(a)** Schematic of our experimental pipeline. DPC, days postconception. **(b)** Volcano plot showing that most DE genes (red) exhibit relatively subtle fold changes (FC). **(c)** *Chd8* is the top differentially expressed gene; panel shows relative expression in *Chd8*^{+/del5} and WT littermates across brain development. DPC, days post conception. **(d)** Example expression patterns in *Chd8*^{+/del5} forebrain of three DE genes across developmental stages. DE FDR shown for **c** and **d**. Solid lines, means; dashed lines, ± 1 s.e.m. **(e)** Validation of DE expression of *Hnrnpa2b1* RNA (left; $n = 6$ WT, 4 *Chd8*^{+/del5}) and protein (right; $n = 5$ WT, 5 *Chd8*^{+/del5}) in *Chd8*^{+/del5} (HT) forebrain at P0 (Student's *t*-test; RNA, $*P = 0.0248$; protein, $**P = 0.0055$). Error bars represent mean \pm s.e.m. **(f)** Chd8 ChIP-seq at *Hnrnpa2b1* and *Adnp* loci. **(g)** Representative significant GO terms for DE genes and for genes whose promoters are bound by Chd8. **(h)** Enrichment of autism-associated genes ($Q < 0.3$ from Sanders *et al.*¹⁹, $P = 2.8 \times 10^{-10}$) in our DE gene set, based on randomly sampled gene sets (bars) vs. observed number (red line). **(i, j)** Comparison of DE down- and upregulated genes identified here with autism- and Chd8-associated genes. Directionality on *x*-axis represents test gene set used in analysis (left of zero: downregulated DE genes; right of zero: upregulated DE genes); *z*-scores generated via permutation test. Vertical lines are at $z = \pm 2$.

After correction for total brain volume, relative volumes were still significantly larger, though cortex failed to surpass the FDR < 5% cut-off (**Fig. 3b**). *Chd8*^{+/del5} mice also displayed increased cortical thickness, particularly along the cingulate cortex (**Fig. 3c**). Deep cerebellar nuclei showed decreased relative volume (-1 to -3% , FDR < 0.3%). Voxel-wise differences showed similar trends (**Fig. 3d**). Diffusion tensor imaging revealed no significant differences in fractional anisotropy or mean diffusivity in either the regional or voxel-wise measurements, indicating that white matter organization and

long-range connectivity in *Chd8*^{+/del5} mice was not grossly different from that in WT littermates (**Supplementary Fig. 3**).

Performing behavioral and structural MRI analyses on the same set of mice allowed us to test correlations between brain volume and behavioral performance. Increased absolute volume of cerebral cortex (f -stat = 33.6, FDR < 0.1%), hippocampus (f -stat = 29.0, FDR < 0.1%) and amygdala (f -stat = 38.6, FDR < 0.1%) were correlated with deficits in learning and memory, as assessed by the context conditioning task (R^2 : cortex = 0.1855, hippocampus = 0.148, amygdala = 0.1352; **Fig. 3e**).

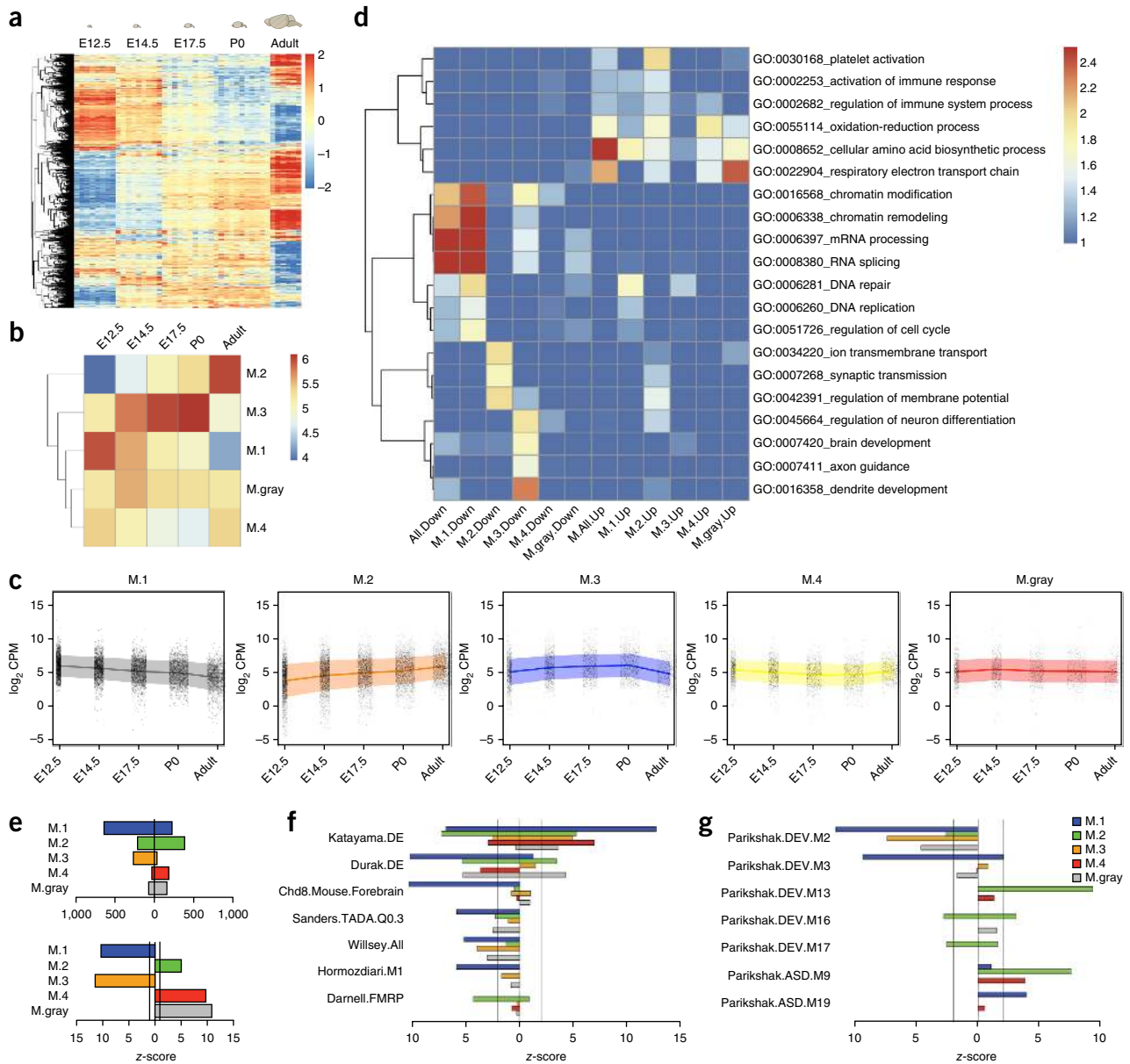


Figure 5 DE genes with correlated expression patterns across brain development reveal perturbations to early and later neurodevelopmental pathways. (a) Heatmap representing expression of DE genes across all samples and stages. Scale bar: z-score. (b) Mean expression across developmental stages for the five developmental gene expression modules. Scale bar, mean $\log_2(\text{CPM})$ of module genes; CPM, counts per million. (c) Gene expression plots for each module. Each plot shows expression for all genes in each module. Line represents mean, shaded area represents ± 1 s.d., and dots depict expression of individual genes. (d) Functional enrichment of representative GO biological process annotations for DE genes. Scale bar, fold enrichment. (e) Top: number of DE genes in each module. Bottom: enrichment of down- or upregulated DE genes per module. (f, g) Enrichment of autism- and *Chd8*-relevant genes within modules. In e–g, directionality on x-axis represents test gene set used in analysis (left of zero: downregulated DE genes; right of zero: upregulated DE genes); z-scores generated via permutation test.

This relationship was driven by *Chd8*^{+/*del5*} mice with increased brain volume. Similar correlations were present between other brain regions and cued and context responses, suggesting that the correlation between fear conditioning performance and brain volume was a general rather than region-specific relationship.

Differential gene expression across neurodevelopment in *Chd8*^{+/*del5*} mice

We applied RNA-seq in forebrain dissected from four developmental stages (E12.5, E14.5, E17.5 and P0) and adult mice (age > P56; Fig. 4a).

This strategy was designed to capture changes during embryonic neurodevelopment but has decreased sensitivity for changes limited to post-natal or adult brains. After quality filtering, we analyzed 26 *Chd8*^{+/*del5*} and 18 WT littermates (sample details in Supplementary Table 2). Using a statistical model that accounted for sex, developmental stage and sequencing batch, we tested for differential expression across 11,936 genes that were robustly expressed in our data sets. At significance cutoffs corresponding to FDR < 0.05 ($P < 0.0021$), FDR < 0.1 ($P < 0.0088$) or FDR < 0.20 ($P < 0.0369$), we found 510, 1,040 and 2,195 genes, respectively, that were differentially expressed (DE; Supplementary Table 3).

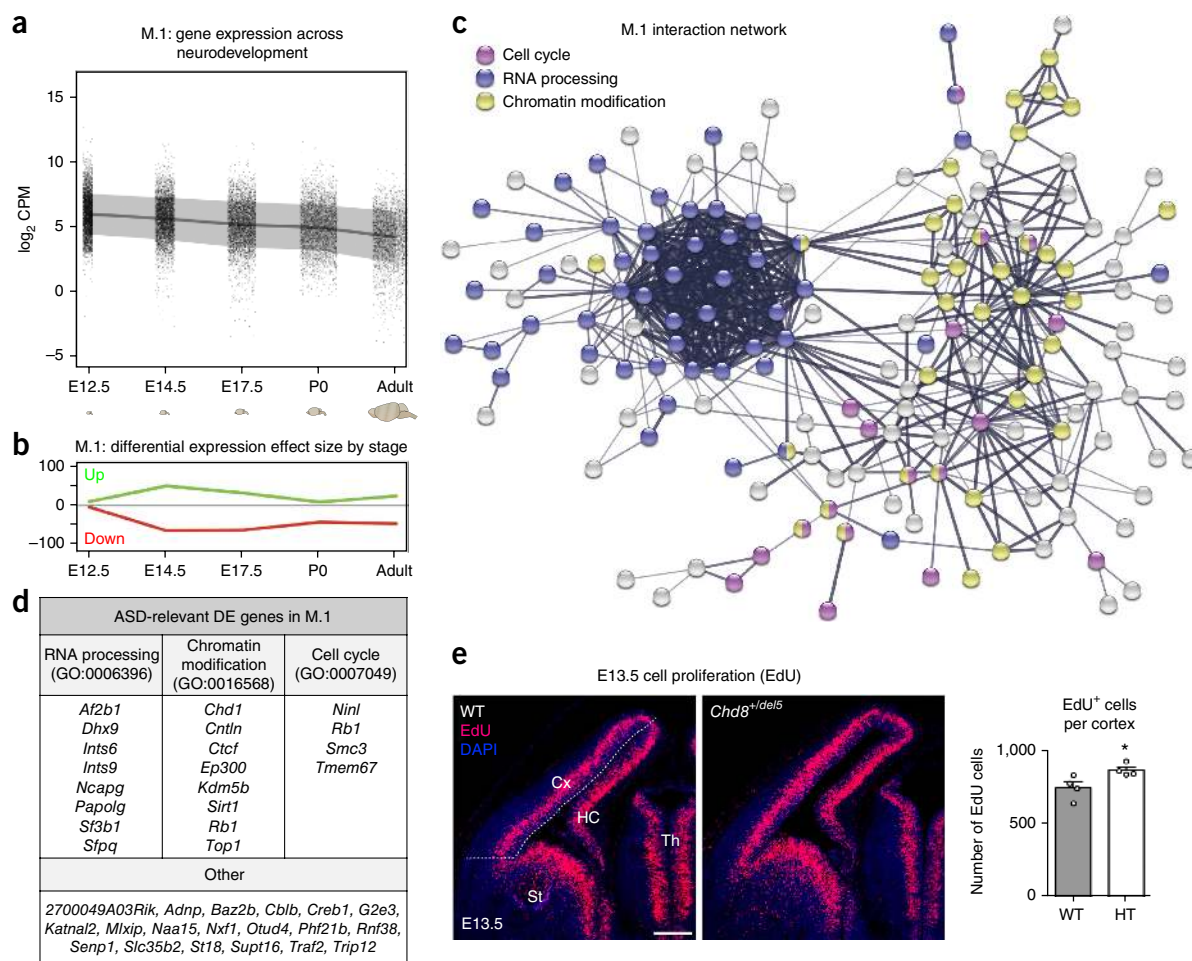


Figure 6 An early neurodevelopmental expression network (M.1) regulated by *Chd8* haploinsufficiency involved in chromatin modification, RNA processing and cell cycle. **(a)** M.1 gene expression plotted across brain development. Dots represent individual genes, line represents mean expression and shaded area represents ± 1 s.d. **(b)** Relative mean differential expression of up- and downregulated genes in M.1 across brain development. **(c)** STRING protein–protein interaction network of M.1. DE genes are colored by annotation to GO biological process terms. **(d)** ASD-relevant DE genes in M.1 associated with selected GO terms. **(e)** Left: representative coronal sections of E13.5 brain stained for EdU (magenta) and DAPI (blue) in WT and *Chd8*^{+/-del5} mice ($n = 4$ mice each for both genotypes). Scale bar, 200 μ m. Below white dotted line is the measured neocortical area. Right: plot (mean \pm s.e.m. with dots representing individual samples) of EdU positive cells per area. Student's *t*-test, $*P = 0.0388$. Cx, cortex; HC, hippocampus; St, striatum; Th, thalamus.

The majority of significant expression changes in *Chd8*^{+/-del5} were relatively small (99.5% < 1.5 absolute fold change across phases; **Fig. 4b**), indicating that changes in neurodevelopmental gene expression were widespread yet subtle. The top DE gene was *Chd8* (\log_2 fold change = 0.59, $P = 2.20 \times 10^{-27}$, FDR = 3.18×10^{-23}). *Chd8* expression declined across development, with substantial reductions in *Chd8*^{+/-del5} mice at each stage (**Fig. 4c**). We validated expression changes at P0 for a set of genes via qRT-PCR (**Supplementary Fig. 4**; primers are listed in **Supplementary Table 4**), including *Hnrnpa2b1*, for which we additionally validated differential protein levels in P0 *Chd8*^{+/-del5} forebrains (**Fig. 4d,e**). Gene set enrichment analysis of Gene Ontology (GO) terms and Reactome¹⁸ pathways identified strong enrichment among DE genes for annotations associated with RNA processing, chromatin remodeling and cell cycle, with numerous additional annotations enriched at lower levels (**Supplementary Tables 5 and 6**). Similar enrichment was observed for DE genes at FDR cutoffs of 0.05, 0.10 and 0.20.

To identify direct regulatory targets of Chd8, we used ChIP-seq to map regions of Chd8 genomic interactions in adult mouse forebrain.

After merging two independent samples with similar binding patterns, we identified 708 peaks using stringent enrichment criteria (**Fig. 4f** and **Supplementary Table 3**). Chd8 binding occurred nearly exclusively at gene promoters in our adult forebrain data set. We observed strong concordance in enriched functional annotation terms between DE and Chd8-bound genes (**Fig. 4g**). While the majority of DE genes did not exhibit Chd8 binding in the adult forebrain Chd8 ChIP-seq generated here, we observed strong enrichment for binding among downregulated genes (**Fig. 4i**). In contrast, we found no enrichment among upregulated DE genes for Chd8 promoter binding. We did not find evidence of a primary sequence motif in Chd8 ChIP-seq peak regions, suggesting indirect genomic recruitment, but we found weaker, yet significant, enrichment of secondary motifs such as YY1 ($e = 4.2 \times 10^{-31}$), NRF1 ($e = 8.5 \times 10^{-24}$) and NFYB ($e = 1.3 \times 10^{-17}$; **Supplementary Fig. 5a**).

In agreement with other studies of transcriptional changes associated with reduction of *Chd8* expression^{11,12}, autism risk genes such as *Kdm5b* and *Bcl11a* were DE in *Chd8*^{+/-del5} mice (**Fig. 4d**). We tested for overlap between DE downregulated and upregulated genes

(FDR < 0.20) and published gene sets relevant to autism genetics and *Chd8* regulation. Of 141 ASD risk genes based on case mutations¹⁹ expressed in our data, 37 were DE at FDR < 0.20 and downregulated, representing strong enrichment (permutation test, $P = 2.8 \times 10^{-10}$; Fig. 4h). We similarly observed enrichment among downregulated DE genes with autism risk genes identified by other studies^{20,21} (Fig. 4i) and with FMRP (fragile X mental retardation protein) targets²² ($P = 0.04$). Finally, we observed enrichment ($P = 0.012$) between DE upregulated genes and genes associated with immune response that were upregulated in cortex from postmortem ASD brains^{23,24}. We did not identify enrichment with genes downregulated in post-mortem ASD cortex.

Next, we asked whether our DE data was consistent with differential expression in independent studies of *Chd8* mutation or knock-down^{11–13,15}. We observed consistent enrichment among up- and downregulated DE genes in *Chd8*^{+/del5} forebrain and up- and downregulated DE genes identified in previous studies (Fig. 4j). We also used the same methods used here to reanalyze neurodevelopmental RNA-seq data from independent studies of germline heterozygous *Chd8* mutation¹³ and *in utero* knockdown via *Chd8* shRNA delivery to E14.5 brain ventricle¹⁵ (Supplementary Fig. 5b,c and Supplementary Table 3). *Chd8* was more strongly downregulated in the knockdown model¹⁵ and upregulated in the independent *Chd8* mouse model¹³. Nonetheless, we observed significant overlap between genes identified here and in the other two studies (Fig. 4j). For overlapping DE genes from our data and the other two studies, DE sensitivity and effect sizes were generally larger in the knockdown data¹⁵ and smaller in the independent germline model¹³ compared to our data (Supplementary Fig. 5b,c), suggesting differences in transcriptional consequences after knockdown and across different alleles or genetic backgrounds. We noted a reversal in direction of some specific DE effects in the knockdown data versus our data, including for neuronal differentiation genes (downregulated here but upregulated after knockdown), further suggesting differential impact of knockdown versus germline mutation.

We next explored how DE genes are organized into expression trajectories during brain development toward identifying perturbation to stage-specific processes. We used weighted gene co-expression network analysis (WGCNA²⁵) to identify five discrete expression trajectory modules across forebrain development (Fig. 5a–c and Supplementary Table 7). DE genes assigned to specific modules were enriched for stage-specific annotation terms (Fig. 5d and Supplementary Table 5). Two modules (M.1 and M.3) were enriched for downregulated genes, while the other three modules (M.2, M.4 and M.grey) were enriched for upregulated genes (Fig. 5e). M.1, characterized by decreasing expression across neurodevelopment, was strongly associated with chromatin organization, RNA processing and cell-cycle regulation, and it included the largest number of DE downregulated autism risk genes (Fig. 5f). M.1 was the only module enriched for targets of *Chd8* binding. M.1 downregulated DE genes overlapped genes in early expressed ASD-relevant networks²⁶ (Parikshak.DEV.M2 and Parikshak.DEV.M3; Fig. 5g). M.2 was characterized by early low expression that gradually increased. Downregulated genes in M.2 were enriched for FMRP targets²², GO and Reactome terms that are hallmarks of mature neurons (Supplementary Tables 5 and 6) and include synaptic genes (Supplementary Fig. 5d) and autism risk genes such as *Cers4* and *Gria1*. DE genes from M.2 were enriched for later developmental ASD-relevant modules²⁶ (Parikshak.DEV.M13, Parikshak.DEV.M16 and Parikshak.DEV.M17) linked to synaptic developmental and homeostatic processes, consistent with developmental timing (Fig. 5g).

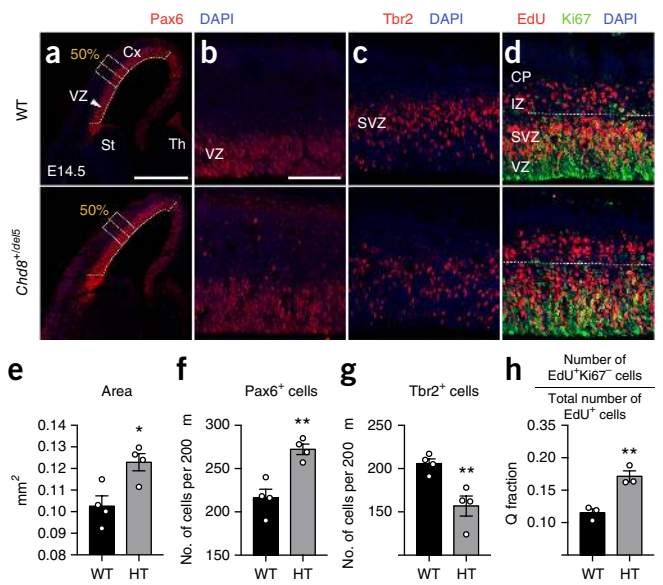


Figure 7 *Chd8*^{+/del5} mutants exhibit altered cortical neurogenesis at E14.5. (a,b) Immunofluorescent analysis of Pax6⁺ radial glial cells reveals an increase in the overall population as measured over the entire cortical hemisphere (a), quantified in e, and within midcortical 200-µm-wide segments (b), quantified in f. Scale bars, 500 µm in a and 100 µm in b–d. (c) Tbr2⁺ intermediate progenitors are significantly reduced, quantified in g. (d,h) The rate of neurogenesis (Q fraction), measured as a ratio of EdU+Ki67⁺ cells positioned basal to the proliferative VZ and SVZ (d; dashed line) over all EdU⁺ cells within the same segment, is increased in *Chd8*^{+/del5} mice (h; 20-h EdU pulse; ** $P = 0.0057$). (e,f) Quantifications of a (* $P = 0.0165$) and b (** $P = 0.0032$), respectively. (g) Quantification of c (** $P = 0.0086$). Analyses performed at E14.5; $n = 4$ mice each for both genotypes in e–g; $n = 3$ mice each for both genotypes in h. All statistics via Student's *t*-test. Error bars represent mean \pm s.e.m. HT, *Chd8*^{+/del5} mice; CP, cortical plate; Cx, cortex; IZ, intermediate zone; LV, lateral ventricle, Str, striatum; SVZ, subventricular zone.

M.3 genes exhibited rising expression from E12.5 to P0, with lower expression in adult brain, were enriched for GO terms associated with transient development processes (for example, axon guidance) and include autism risk genes involved in neuronal maturation (for example, *Bcl11a*). Compared to genes identified as DE in postmortem ASD cortex²⁴, we identified enrichment with two modules characterized by increased expression of genes linked to immune function and cell identity of astrocytes (Parikshak.ASD.M9, enriched for upregulated genes in our M.2 and M.4) or microglia (Parikshak.ASD.M19, enriched for upregulated genes in our M.1; Fig. 5g). These results show that the impact of *Chd8* haploinsufficiency reaches across stages and biological processes.

We further focused on M.1, which showed the strongest enrichment for autism risk early developmental modules²⁶ and for *Chd8* binding targets in mouse brain (Fig. 5f,g). M.1 showed a general trend of decreasing expression (Fig. 6a), had the greatest number of DE genes and was significantly enriched for downregulated genes ($P = 8.8 \times 10^{-26}$). We found 865 genes in M.1 that were DE at FDR < 0.20 (641 downregulated, 224 upregulated), accounting for ~39% of all DE genes identified in our study. Upregulation of M.1 genes peaked at E14.5; downregulation peaked from E14.5 to E17.5 (Fig. 6b). Analysis of protein–protein interactions (STRING²⁷) showed that DE (FDR < 0.10) genes in M.1 had more interactions than expected by chance (observed edges = 1,479, expected edges = 512, enrichment = 2.89, STRING $P < 0.0001$). Interacting genes in M.1 were enriched for GO terms

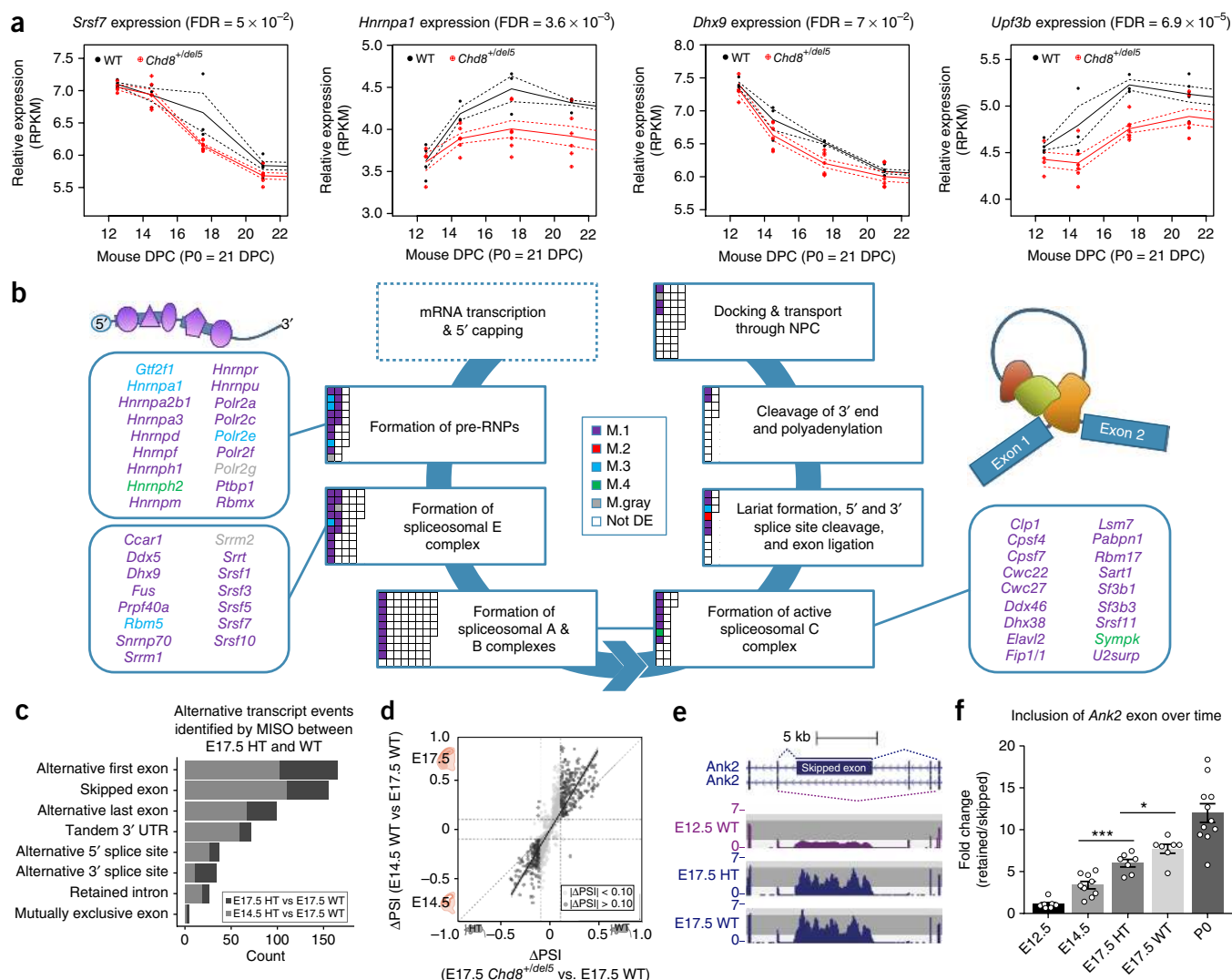


Figure 8 RNA processing pathways are enriched for differentially expressed genes in *Chd8*^{+/-del5} mice. (a) Developmental expression of DE genes annotated to the formation of pre-mRNPs (*Hnnpa1*), formation of the spliceosomal E complex (*Srsf7* and *Dhx9*), and lariar formation and 5' splice site cleavage (*Upf3b*). DE FDR shown; RPKM, reads per kilobase of transcript per million mapped reads. Solid lines, means; dashed lines, \pm s.e.m. (b) Schematic of the Reactome RNA-processing pathways. DE genes in the pathways are denoted as squares colored by module. Each gene is represented once. Images depict simplified schematics of nascent pre-mRNA (top left) and the active spliceosomal C complex (top right). (c) We detected 591 differential isoforms (dark gray) by MISO between E17.5 *Chd8*^{+/-del5} and E17.5 WT brains. Of these, 393 isoforms were also differentially spliced between E14.5 WT vs. E17.5 WT (light gray). (d) Scatterplot of change in percentage spliced in (Δ PSI) of isoforms detected between E17.5 *Chd8*^{+/-del5} (HT) vs. E17.5 WT (dark gray) and E14.5 WT vs. E17.5 WT (light gray) comparisons, showing strong correlation between genotype and developmental events and direction of splicing change. (e) Genome Browser representation of the alternatively spliced *Ank2* exon (chr3:126,644,528–126,650,725). (f) Isoform-specific qRT-PCR of the *Ank2* exon in WT and E17.5 *Chd8*^{+/-del5} mice ($n = 7$ E12.5, 9 E14.5, 7 E17.5 *Chd8*^{+/-del5}, 7 E17.5 WT, 11 P0 mice; Welch's t -test, E14.5 WT vs. E17.5 *Chd8*^{+/-del5}, *** $P = 0.001$; E17.5 *Chd8*^{+/-del5} vs. E17.5 WT, * $P = 0.03$). Linear regression across developmental time points, adjusted $R^2 = 0.77$, $P = 4.53 \times 10^{-14}$. Error bars represent mean \pm s.e.m.

including RNA processing, chromatin modification and cell cycle (Fig. 6c). While protein-protein interaction databases have biases, these results highlight interconnectedness among these three processes at the level of *Chd8* regulation and gene expression. M.1 DE genes include 38 autism-relevant genes, including many annotated to the highlighted GO terms (Fig. 6d).

Increased prenatal proliferation of neural progenitors in *Chd8*^{+/-del5} mice

To examine whether alterations in developmental genes play a functional role in neuronal development that could lead to megalencephaly,

we performed 5-ethynyl-2'-deoxyuridine (EdU) proliferation assays at E13.5. After a 1.5-h pulse, we observed a 15.9% increase in EdU⁺ cells in the germinal cortical ventricular and subventricular zones (VZ and SVZ, respectively) of mutant animals ($P = 0.0388$; Fig. 6e), indicating perturbed neurogenesis in the *Chd8*^{+/-del5} mutants. Additionally, since a number of genes associated with brain development and cortical structure were DE, we examined the cortical cytoarchitecture via analysis of layer-specific markers *Tbr1*, *Ctip2* and *Brn2* by immunostaining at P0 and P7 (Supplementary Fig. 6). We observed no gross alterations to lamination and found no evidence for focal cortical lesions. To further delineate proliferative changes in

Chd8^{+/*del5*} mice, we assessed neural progenitor populations at E14.5 (Fig. 7). First, we examined Pax6⁺ radial glial cells, measuring VZ area over the entire cortical hemisphere. The VZ in *Chd8*^{+/*del5*} embryos was significantly increased, by ~18% (Fig. 7a,e; $P = 0.0165$). We observed a ~26% increase in Pax6⁺ cells in *Chd8*^{+/*del5*} brains (Fig. 7b,f; $P = 0.0032$). Subsequently, we labeled Tbr2⁺ intermediate progenitors, observing a significant decrease by ~24% in *Chd8*^{+/*del5*} mice (Fig. 7c,g; $P = 0.0086$), indicating different proliferative trajectories for these two progenitor types. Finally, we performed pulse-chase assays to determine the quit (Q) fraction of cortical cells exiting the cell cycle over a defined 20 h, using the proliferation marker Ki67. EdU⁺Ki67⁻ cells were significantly increased, corresponding to an increase in Q fraction by ~25% in *Chd8*^{+/*del5*} embryos (Fig. 7d,h; $P = 0.0057$). These results indicate that alteration to cortical projection neuron production may represent a cellular substrate for megalencephaly in *Chd8*^{+/*del5*} mice.

Neurodevelopmental RNA processing is perturbed in *Chd8*^{+/*del5*} mice

Downregulated DE genes with divergent expression trajectories were significantly overrepresented among genes annotated to RNA processing and mRNA splicing in the Reactome database (Fig. 8a,b and Supplementary Table 6). For example, *Dhx9* (M.1) decreases across neurodevelopment and has not been functionally characterized in brain but has been reported in autism risk networks²⁰, while *Upf3b* (M.3) expression increases across development and is a neuron-specific factor required during neuronal differentiation that is implicated in ID^{28,29}. We examined whether *Chd8*^{+/*del5*} mice exhibited aberrant splicing during brain development linked to DE of RNA-processing genes. We used the Mixture of Isoforms (MISO³⁰) program to examine our RNA-seq data for differential splicing (DS) between WT and *Chd8*^{+/*del5*} mice and across neurodevelopment in WT mice (Supplementary Table 8). Genes associated with a DS event in *Chd8*^{+/*del5*} mice significantly overlapped downregulated ($P = 1.2 \times 10^{-10}$) but not upregulated DE genes, raising the possibility that splicing changes explain some proportion of differential expression (Supplementary Fig. 7a). DS genes identified in *Chd8*^{+/*del5*} mouse brain were enriched for DS-associated genes identified in post-mortem ASD cortex²⁴ ($P = 1.2 \times 10^{-17}$), suggesting that DS in *Chd8*^{+/*del5*} mice is linked to ASD-relevant DS (Supplementary Fig. 7a).

At E17.5, MISO identified 591 DS events between WT and *Chd8*^{+/*del5*} mice, of which 393 (~66%) were also DS between E14.5 WT and E17.5 WT mice (Fig. 8c). These results suggest that differential splicing between WT and *Chd8*^{+/*del5*} mice was linked to developmental changes in splicing. To investigate this, we examined correlation between DS events present in both E14.5 WT versus E17.5 WT and E17.5 *Chd8*^{+/*del5*} versus E17.5 WT comparisons. Percentage spliced in (PSI) values of DS events identified in the E17.5 *Chd8*^{+/*del5*} versus E17.5 WT comparison correlated positively with PSI values in the E14.5 WT versus E17.5 WT comparison (Fig. 8d). This correlation suggests DS in E17.5 *Chd8*^{+/*del5*} mice corresponds to an intermediate developmental state between WT E14.5 and E17.5. We validated developmentally relevant *Chd8*^{+/*del5*} DS using a known neurogenic splicing event, inclusion or exclusion of a ~6-kb *Ank2* exon³¹. Inclusion of the *Ank2* exon increased between E12.5 and E17.5 in WT (Fig. 8e), consistent with expectations³¹. qRT-PCR analysis of the *Ank2* exon validated the exon inclusion increase across development in WT and the decrease from E17.5 WT levels in E17.5 *Chd8*^{+/*del5*} mice (Fig. 8f). We also validated developmental splicing changes in *Srsf7* detected via MISO analysis (Supplementary Fig. 7b). Our results suggest that perturbed splicing in *Chd8* haploinsufficiency may contribute to the neurodevelopmental phenotypes in *Chd8*^{+/*del5*} mice.

DISCUSSION

Modeling how constitutive heterozygous germline mutations impact mammalian brain development is critical to understanding the neurobiology of disorders like ASD and ID, which are strongly associated with single-copy loss-of-function mutations. After validation that germline 5-bp and 14-bp deletion mutations in *Chd8* exon 5 resulted in haploinsufficiency, we present here an initial integrative picture of the consequences of *Chd8* haploinsufficiency on neurodevelopment. The presence of genomic and neuroanatomical phenotypes in our *Chd8*^{+/*del5*} mice paralleled the clinical signature of human *CHD8* mutations, suggesting similar neurodevelopmental pathologies between species. Our study revealed NDD-relevant phenotypes and mechanistic insights into why haploinsufficiency of a general chromatin factor produces neurodevelopmental phenotypes.

We report behavioral outcomes in our heterozygous *Chd8*^{+/*del5*} mice, specifically learning and memory impairments, but no atypical sociability or repetitive behaviors. There are three recent publications associated with downregulation of *Chd8* in mice. Durak *et al.*¹⁵ reported an *in utero* knockdown of *Chd8* expression, including restricted knockdown of *Chd8* in upper cortical layer neurons. Katayama *et al.*¹³ generated two lines of *Chd8* mutant mice via embryonic stem cell targeting, while Platt *et al.*¹⁴ used CRISPR/Cas9 targeting to generate indel mutations in *Chd8*. The obvious differences in biological consequences and mechanisms between *in utero* knockdown¹⁵ and our germline heterozygous model likely explain many differences and make cross-approach comparisons a challenge. Our data on the absence of repetitive behaviors agree with those reported in Katayama *et al.*¹³ and Platt *et al.*¹⁴; however, these studies also report specific social phenotypes in heterozygous *Chd8* mice. We focus our comparison on the Katayama *et al.*¹³ study as we were able to directly compare neurodevelopmental gene expression changes to our model. We observed differences in strength of expression changes that may be due to allele or genetic background. Katayama *et al.*¹³ report phenotypes relevant to social deficits but report normal acquisition learning using the Barnes and T-maze assays. Discrepancies in cognitive phenotypes could be attributed to the tasks conducted, since spatial maze tasks are primarily hippocampal-dependent, while components of fear conditioning and novel object recognition require other brain regions, including amygdala. Additionally, our *Chd8*^{+/*del5*} mutation was generated and maintained on a C57BL/6N background, while Katayama *et al.*¹³ harbored a different mutation on C57BL/6J. Background strain differences in behavioral phenotypes are common, and C57BL/6N generally show higher basal freezing during contextual fear freezing, which allows for a larger signal and detection of genotype differences³².

Our finding of normal sociability is consistent with results reported for other *Chd8*^{+/-} germline models^{13,14}. However, both other models^{13,14}, report abnormalities in social behavior based on failure of *Chd8*^{+/-} mice to exhibit preference for social novelty between a novel and familiar mouse. Preference for social novelty is dependent on olfactory discrimination, which is driven by a variety of sensory and processing systems. As such, the combination of normal three-chamber assay sociability but failure to discriminate a novel mouse in these models^{13,14} could represent mild deficits in social interaction or could be due to other factors impacting olfactory discrimination. Another difference is that Katayama *et al.*¹³ tested only male mice with a broad age range of 12–50 weeks of age, while our battery was conducted using both sexes at younger ages, between 6–16 weeks, to avoid aging as a confounding variable. We also note that several studies of other mouse models with mutations in genes implicated in ASD have not identified deficits in social

behaviors³³, potentially due to evolutionary divergence between mouse and human neurobiology, allele or genetic background differences, or sensitivity of methods used to evaluate ASD-relevant behavior in mice.

The structural changes in the brain of adult *Chd8*^{+/*del5*} mice observed here parallel those found in other relevant mouse models. A recent study examined 26 different mouse models related to autism³⁴, clustering these models into three distinct groups. Key aspects of Group 1 included larger cortical structures, particularly the frontal and parietal lobes, and smaller structures in the cerebellum, which is in line with the *Chd8*^{+/*del5*} mouse described here. This group of models included *Nrxn1α*, *Shank3*, *En2* and *Fmr1* mutants. The *Chd8*^{+/*del5*} mouse most resembled the differences found in the *Fmr1* mutant mice. Further examination may reveal similarities with other mouse models within this group beyond neuroanatomy (for example, excitatory deficits in the *Nrxn1α* mouse³⁵), as suggested by the widespread transcriptional changes present in *Chd8*^{+/*del5*} neurodevelopment. Increases in cortical anteroposterior length and developmental neurogenesis appear largely overlapping in *Chd8*^{+/*del5*} mice and *Wdly3* mutants, another model of megalencephaly in ASD³⁶. Future work will be needed to test for causal relationships between structural changes and behavior in *Chd8*^{+/*del5*} mice.

Our RNA-seq analysis captured subtle changes in transcription across brain development in *Chd8*^{+/*del5*} mice, as well as evidence of differential splicing. Differential expression changes were consistent across developmental stages for perturbed genes highly relevant to ASD-associated networks and strongly correlated with biological pathways and expression modules of interest. Our network analysis, using *in vivo* data, enabled characterization of the impact of *Chd8* haploinsufficiency across neurodevelopment at a level of detail sufficient to capture perturbations across developmental stages and processes. Our results indicate convergent neuropathology connecting principle gene networks identified in ASD case sequencing studies, particularly chromatin remodeling, neuronal differentiation and synaptic pathways^{7,8}, and those identified in other ASD-relevant pathways such as immune response²⁴ and FMRP binding²². Our findings suggest a hierarchy of changes in *Chd8*^{+/*del5*} brain development anchored by dysregulation of genes in M.1, which represents a highly interactive network central to control of chromatin state, RNA processing and cell cycle, including numerous genes implicated in ASD. Among these genes, our results suggest direct role and requirement for WT *Chd8* expression levels in activating target gene expression. As seen with other NDD genetic models such as *Fmr1* (ref. 37) and *Rbfox1* (ref. 38), disruption to RNA processing, likely driven by indirect transcriptional regulation here, appears to be an important player in *Chd8*^{+/*del5*} neuropathology. Further studies are needed to capture neuroanatomical and cellular changes associated with differential expression signatures and to determine stage- and cell-specific patterns and roles of *Chd8* binding. This is especially critical given that contrasting *Chd8* genomic interaction patterns have been reported in brain^{11–14}.

We report overall increased proliferation during the peak window of embryonic neurogenesis, with different consequences for the progenitor populations involved. The observed overall increase in proliferation in our experiments contrasts with the decreased proliferation reported in an *in utero* *Chd8* knockdown model¹⁵. These differences could be explained by the timing of *in utero* knockdown at E14.5 (after initial symmetric expansion of the radial glia pool), by the presence of non-cell-autonomous effects or due to differences in proliferation assay timing. Time-point-specific analysis of cell cycle, proliferation and apoptosis will be needed to understand the comprehensive impact of *Chd8* haploinsufficiency on cell populations in the brain. It is possible

that contrasting outcomes are due to differences in *Chd8* dosage, considering that knockdown resulted in greater *Chd8* downregulation¹⁵. As complete *Chd8* loss impedes embryonic development at very early stages¹⁰, downregulation beyond haploinsufficiency may interfere further with developmental cellular pathways. In support of this, neuronal development genes downregulated in our M.3 module were upregulated after *in utero* knockdown, suggesting that knockdown caused an early shift from proliferation to differentiation¹⁵ that did not appear to occur with heterozygous germline mutation.

Our initial survey of mice heterozygous for mutation to *Chd8* revealed significant findings across genomic, anatomical and behavioral axes of neurobiology. Our experiments link cognitive deficits, increased regional brain volume and perturbations of biological pathways across neurodevelopment, recapitulating traits observed in human individuals who carry mutations in *CHD8*. The transcription data generated here represent a resource for dissecting the pathways involved in NDD pathogenesis and for prioritizing risk genes from genetic studies. Additional studies will be necessary to replicate and compare findings across mutant *Chd8* alleles and genetic backgrounds and to clarify dosage-specific phenotypes. Our results offer insight into neurodevelopmental pathology associated with mutations to *CHD8*, a genetic model that appears to be a bellwether for mutations affecting chromatin remodeling in autism.

METHODS

Methods, including statements of data availability and any associated accession codes and references, are available in the [online version of the paper](#).

Note: Any Supplementary Information and Source Data files are available in the online version of the paper.

ACKNOWLEDGMENTS

Sequencing was performed at the UC Berkeley and UC Davis DNA cores. This work was supported by institutional funds from the UC Davis Center for Neuroscience, by the UC Davis MIND Institute Intellectual and Developmental Disabilities Research Center (U54 HD079125) and by NIGMS R35 GM119831. L.S.-F. was supported by the UC Davis Floyd and Mary Schwall Fellowship in Medical Research and by grant number T32-GM008799 from NIGMS-NIH. A.A.W. was supported by Training Grant number T32-GM007377 from NIH-NIGMS. R.C.-P. was supported by a Science Without Borders Fellowship from CNPq (Brazil). A.V., L.A.P. and D.E.D. were supported by National Institutes of Health grants R24HL123879, U01DE024427, R01HG003988, U54HG006997 and UM1HL098166. Research conducted at the E.O. Lawrence Berkeley National Laboratory was performed under Department of Energy Contract DE-AC02-05CH11231, University of California. J.E. and J.P.L. were supported by the Canadian Institute for Health Research, Brain Canada and the Ontario Brain Institute.

AUTHOR CONTRIBUTIONS

A.L.G., L.S.-F., J.E., N.A.C. and M.A.R. are listed as joint first authors, as each led components of the experiments and analysis. A.L.G., L.S.-F., J.E., M.A.R., N.A.C., J.P.L., J.N.C., J.L.S., K.S.Z. and A.S.N. designed the experiments. Generation of mouse model: A.S.N., D.E.D., A.V., L.A.P., B.J.M., I.P.-F. and V.A.; mouse behavior: N.A.C., M.C.P., M.D.S., J.N.C. and J.L.S.; mouse MRI: J.E. and J.P.L.; genomics and molecular genetics: L.S.-F., A.L.G., I.Z., A.A.W., R.C.-P., S.L., B.J.M. and A.S.N.; neuroanatomy: A.L.G., M.A.R., T.W.S., I.Z., G.K., K.S.Z. A.L.G., L.S.-F., J.E., N.A.C., M.A.R., K.S.Z., J.N.C., J.L.S. and A.S.N. drafted the manuscript. All authors contributed to manuscript revisions.

COMPETING FINANCIAL INTERESTS

The authors declare no competing financial interests.

Reprints and permissions information is available online at <http://www.nature.com/reprints/index.html>. Publisher's note: Springer Nature remains neutral with regard to jurisdictional claims in published maps and institutional affiliations.

1. Ho, L. & Crabtree, G.R. Chromatin remodelling during development. *Nature* **463**, 474–484 (2010).
2. Chen, T. & Dent, S.Y.R. Chromatin modifiers and remodellers: regulators of cellular differentiation. *Nat. Rev. Genet.* **15**, 93–106 (2014).

3. Ronan, J.L., Wu, W. & Crabtree, G.R. From neural development to cognition: unexpected roles for chromatin. *Nat. Rev. Genet.* **14**, 347–359 (2013).
4. Sanders, S.J. First glimpses of the neurobiology of autism spectrum disorder. *Curr. Opin. Genet. Dev.* **33**, 80–92 (2015).
5. McCarthy, S.E. *et al.* *De novo* mutations in schizophrenia implicate chromatin remodeling and support a genetic overlap with autism and intellectual disability. *Mol. Psychiatry* **19**, 652–658 (2014).
6. Vissers, L.E.L.M., Gilissen, C. & Veltman, J.A. Genetic studies in intellectual disability and related disorders. *Nat. Rev. Genet.* **17**, 9–18 (2016).
7. De Rubeis, S. *et al.* Synaptic, transcriptional and chromatin genes disrupted in autism. *Nature* **515**, 209–215 (2014).
8. Iossifov, I. *et al.* The contribution of *de novo* coding mutations to autism spectrum disorder. *Nature* **515**, 216–221 (2014).
9. Bernier, R. *et al.* Disruptive *CHD8* mutations define a subtype of autism early in development. *Cell* **158**, 263–276 (2014).
10. Nishiyama, M. *et al.* Early embryonic death in mice lacking the beta-catenin-binding protein Duplin. *Mol. Cell. Biol.* **24**, 8386–8394 (2004).
11. Sugathan, A. *et al.* *CHD8* regulates neurodevelopmental pathways associated with autism spectrum disorder in neural progenitors. *Proc. Natl. Acad. Sci. USA* **111**, E4468–E4477 (2014).
12. Cotney, J. *et al.* The autism-associated chromatin modifier *CHD8* regulates other autism risk genes during human neurodevelopment. *Nat. Commun.* **6**, 6404 (2015).
13. Katayama, Y. *et al.* *CHD8* haploinsufficiency results in autistic-like phenotypes in mice. *Nature* **537**, 675–679 (2016).
14. Platt, R.J. *et al.* *Chd8* Mutation Leads to autistic-like behaviors and impaired striatal circuits. *Cell Rep.* **19**, 335–350 (2017).
15. Durak, O. *et al.* *Chd8* mediates cortical neurogenesis via transcriptional regulation of cell cycle and Wnt signaling. *Nat. Neurosci.* **19**, 1477–1488 (2016).
16. Silverman, J.L., Yang, M., Lord, C. & Crawley, J.N. Behavioural phenotyping assays for mouse models of autism. *Nat. Rev. Neurosci.* **11**, 490–502 (2010).
17. Silverman, J.L., Babineau, B.A., Oliver, C.F., Karras, M.N. & Crawley, J.N. Influence of stimulant-induced hyperactivity on social approach in the BTBR mouse model of autism. *Neuropharmacology* **68**, 210–222 (2013).
18. Croft, D. *et al.* The Reactome pathway knowledgebase. *Nucleic Acids Res.* **42**, D472–D477 (2014).
19. Sanders, S.J. *et al.* Insights into autism spectrum disorder genomic architecture and biology from 71 risk loci. *Neuron* **87**, 1215–1233 (2015).
20. Hormozdiari, F., Penn, O., Borenstein, E. & Eichler, E.E. The discovery of integrated gene networks for autism and related disorders. *Genome Res.* **25**, 142–154 (2015).
21. Willsey, A.J. *et al.* Coexpression networks implicate human midfetal deep cortical projection neurons in the pathogenesis of autism. *Cell* **155**, 997–1007 (2013).
22. Darnell, J.C. *et al.* FMRP stalls ribosomal translocation on mRNAs linked to synaptic function and autism. *Cell* **146**, 247–261 (2011).
23. Voineagu, I. *et al.* Transcriptomic analysis of autistic brain reveals convergent molecular pathology. *Nature* **474**, 380–384 (2011).
24. Parikhshak, N.N. *et al.* Genome-wide changes in lncRNA, splicing, and regional gene expression patterns in autism. *Nature* **540**, 423–427 (2016).
25. Langfelder, P. & Horvath, S. WGCNA: an R package for weighted correlation network analysis. *BMC Bioinformatics* **9**, 559 (2008).
26. Parikhshak, N.N. *et al.* Integrative functional genomic analyses implicate specific molecular pathways and circuits in autism. *Cell* **155**, 1008–1021 (2013).
27. Jensen, L.J. *et al.* STRING 8—a global view on proteins and their functional interactions in 630 organisms. *Nucleic Acids Res.* **37**, D412–D416 (2009).
28. Alrabhani, T. *et al.* Full *UPF3B* function is critical for neuronal differentiation of neural stem cells. *Mol. Brain* **8**, 33 (2015).
29. Laumonnier, F. *et al.* Mutations of the *UPF3B* gene, which encodes a protein widely expressed in neurons, are associated with nonspecific mental retardation with or without autism. *Mol. Psychiatry* **15**, 767–776 (2010).
30. Katz, Y., Wang, E.T., Airoidi, E.M. & Burge, C.B. Analysis and design of RNA sequencing experiments for identifying isoform regulation. *Nat. Methods* **7**, 1009–1015 (2010).
31. Zhang, X. *et al.* Cell-type-specific alternative splicing governs cell fate in the developing cerebral cortex. *Cell* **166**, 1147–1162.e15 (2016).
32. Tipps, M.E., Raybuck, J.D., Buck, K.J. & Lattal, K.M. Delay and trace fear conditioning in C57BL/6 and DBA/2 mice: issues of measurement and performance. *Learn. Mem.* **21**, 380–393 (2014).
33. Brunner, D. *et al.* Comprehensive analysis of the 16p11.2 deletion and null *Cntnap2* mouse models of autism spectrum disorder. *PLoS One* **10**, e0134572 (2015).
34. Ellegood, J. *et al.* Clustering autism: using neuroanatomical differences in 26 mouse models to gain insight into the heterogeneity. *Mol. Psychiatry* **20**, 118–125 (2015).
35. Etherton, M.R., Blaiss, C.A., Powell, C.M. & Südhof, T.C. Mouse neurexin-1 α deletion causes correlated electrophysiological and behavioral changes consistent with cognitive impairments. *Proc. Natl. Acad. Sci. USA* **106**, 17998–18003 (2009).
36. Orosco, L.A. *et al.* Loss of *Wdfy3* in mice alters cerebral cortical neurogenesis reflecting aspects of the autism pathology. *Nat. Commun.* **5**, 4692 (2014).
37. Hagerman, R., Au, J. & Hagerman, P. FMR1 premutation and full mutation molecular mechanisms related to autism. *J. Neurodev. Disord.* **3**, 211–224 (2011).
38. Lee, J.-A. *et al.* Cytoplasmic Rbfox1 regulates the expression of synaptic and autism-related genes. *Neuron* **89**, 113–128 (2016).

ONLINE METHODS

Generation of *Chd8* mutant mice. We used Cas9-mediated mutagenesis of C57BL/6N oocytes to generate two mouse lines harboring frameshift deletions (5 bp and 14 bp) in mouse *Chd8* exon 5. Guide RNA was designed and synthesized according to described methods³⁹, pooled with Cas9 mRNA and injected into mouse oocytes. We scanned the *Chd8* coding sequence for unique gRNA target sites, identifying one in exon 5 with sequence GAGGAGGAGGTCGATGTAAC. This sequence maps uniquely to the target site via BLAT (mm9), reducing the likelihood of off-target mutations. Initial Cas9 targeting was performed at Lawrence Berkeley National Laboratory. F0s (induced on C57BL/6N background) carrying mutations were genotyped and bred to expand lines that harbored a mutation. We identified F0 pups carrying 5-bp (mm9: chr14:52,847,259–52,847,263) and 14-bp deletions (mm9: chr14:52,847,249–52,847,262) in *Chd8* exon 5 that overlapped the target sequence. The deletions occur at position 1,814 (5-bp deletion) or 1,813 (14-bp deletion) of *Chd8* mRNA (uc007tot.1). Both alleles match wild-type *Chd8* amino acid sequence through position 604, after which the 5-bp and 14-bp deletion frameshifts are predicted to result in 16 and 14 altered amino acids, respectively, before a stop codon is reached. The full-length *Chd8* protein is predicted to be 2,582 amino acids. Both deletion alleles are predicted to result in nonsense-mediated decay based on reduced frequency of mutant transcripts and decreased *Chd8* protein levels. Deletion alleles were subcloned to verify DNA changes, and genotyping was performed using allele-specific PCR with sequence verification.

The colony of animals carrying the 5-bp *Chd8* deletion allele was rederived at UC Davis and maintained by crossing male carriers with C57BL/6N wild-type females (Charles River). Extensive crossing of heterozygous mutation carriers to wild-type animals vastly reduces the likelihood that any potential off-target mutations caused by Cas9 targeting would persist in our mutant *Chd8* line. Genotypes were identified via allele-specific PCR and sequence-verified for all animals included in analyses, with the primers reported in **Supplementary Table 4**. We examined *Chd8* protein and transcript levels via western blot and qRT-PCR at E14.5 and P0 and compared cortical length in whole-mount P0 brains from *Chd8^{+/-del5}* mice and matched WT littermates. For all experiments, samples from both males and females were used unless otherwise described. All mouse studies were approved by the Institutional Animal Care and Use Committees at the University of California Davis and the Lawrence Berkeley National Laboratory. Subject mice were housed in a temperature-controlled vivarium maintained on a 12-h light–dark cycle. Efforts were made to minimize pain and distress and the number of animals used.

qRT-PCR. Differential expression of selected gene targets was verified by qRT-PCR at P0, using cDNA libraries prepared following the same protocols listed in the “Genomics” section, below. Primers are reported in **Supplementary Table 4**. For qRT-PCR analysis, $n = 9$ WT and 7 *Chd8^{+/-del5}* forebrains from male and female samples were used. Samples were excluded if technical replicates failed. Cycle counts were normalized to *Actb*. Unpaired *t*-tests were performed on normalized relative gene expression between WT and *Chd8^{+/-del5}* brains using $\Delta\Delta CT$. To reduce noise, the highest and lowest values from both groups were discarded. To validate differential splicing, we used isoform-specific quantitative reverse-transcription PCR on cDNA libraries prepared from forebrains dissected from *Chd8^{+/-del5}* and matched WT littermates. We used primers validated for isoform analysis of *Ank2* expression during development³¹ and designed primers specific to a differentially spliced exon of *Srsf7*. Comparisons of splicing across stages and between *Chd8^{+/-del5}* and matched WT littermates were analyzed using Welch's *t*-test and linear regression.

Western blot analysis. Isolated forebrain from E14.5 embryos (male and female littermates), P0 neonates and P60 adults were lysed in 50 mM Tris HCl, pH 8, 140 mM NaCl, 1 mM EDTA, 10% glycerol, 0.5% NP40 and 0.25% Triton with protease inhibitor cocktail (Roche). After sonication, samples were spun down and the supernatant was used for a BCA Bradford assay using the Spectramax 190 plate reader to assess protein concentration using a standard curve. We ran 22 μ g of protein on a 3–8% Tris acetate gel using the Novex western blotting system (Invitrogen). Anti-*Chd8* (ref. 12) (1:1,000, ab114126; Abcam), anti-Hnrnpa2b1 (ref. 40) (1:1,000, ab31645; Abcam) and anti-Gapdh (ref. 41) (1:10,000, G8795; Sigma-Aldrich) primary antibodies were incubated overnight in Fluorescent Blocker solution (Millipore), visualized using a LI-COR Odyssey CLx system and quantified in FIJI (National Institutes of Health). For *Chd8* western blots,

both males and females were used. For the Hnrnpa2b1 western blot, only male samples were used. Protein levels assayed via western blot were compared via Student's *t*-test and one-way ANOVA for adult *Chd8* levels.

Analysis of cortical length at P0. For gross anatomical measurements at P0 and P7, *Chd8* male and female littermates were decapitated and heads placed in 4% PFA for at least 24 h. Brains were carefully dissected and placed in an agarose mold to ensure specific positioning. Whole-mount images were taken with the Zeiss Lumar.V12 stereoscope with a Ned Lumar 0.8 \times FwD 80-mm objective and Axiovision 4.8 software. Analysis of cortical length measurements was performed with FIJI software (National Institutes of Health).

Morphological analysis. All histological experiments were performed at least in triplicate on embryos/pups from at least two separate litters. Following anesthesia, P7 male and female mice were transcardially perfused with 4% paraformaldehyde (PFA) in phosphate-buffered saline (PBS), followed by overnight fixation in the same solution. After fixation, brains were removed from the skull, embedded in 2% LTE Agarose/PBS and cut coronally in 50- μ m sections on a vibratome (VT 1000S, Leica). Subsequently, the sections were mounted on glass slides (SuperFrost Plus, Thermo-Fisher), Nissl-stained with a 0.1% cresyl violet solution and mounted with DePeX (Electron Microscopy Sciences, Hatfield, PA). Select sections, approximately corresponding to adult bregma -2 mm, were aligned across genotypes using subcortical anatomical landmarks for orientation (hippocampal length, thalamic size), and images of entire hemispheres were acquired on a Keyence BZ microscope. We measured individual morphological parameters using the Keyence BZ analyzer (hemispheric/neocortical circumference, neocortical thickness) or FIJI software (cortical area). Hemispheric circumferences were measured from the dorsal to the ventral midline. Neocortical circumferences were measured from the dorsal midline to a line perpendicular to the midline originating from the dorsal endpoint of the dorsal endopiriform nucleus.

EdU labeling and immunofluorescent analysis. Litters for neuroanatomy analysis were generated by breeding male *Chd8^{+/-del5}* mice with WT females. Brains were perfused before isolation, embedding and sectioning. Experimenters were blinded to genotype. Both male and female samples were used in the following assays.

Time-pregnant females were intraperitoneally injected at E13.5 with 50 mg/kg body weight EdU. After 1.5 h (proliferation assay) or 20 h (Q-fraction analysis), females were anesthetized and embryos transcardially perfused with 4% PFA/PBS. After 2 h of further fixation in the same solution, embryo brains were immersed in 15% and then 30% sucrose in PBS, placed in OCT compound (Fisher HealthCare, Houston, TX), frozen in dry-ice-chilled methanol and sectioned at 16 μ m (1.5-h pulse) or 18 μ m (20-h pulse) on a cryostat (Leica Biosystems, Buffalo Grove, IL). EdU detection was performed with the Click-iT EdU Alexa Fluor 594 imaging kit protocol (Life Technologies, Carlsbad, CA) according to the manufacturer's instructions. Q-fraction analysis followed previously established practices³⁶. In brief, midcortical 200- μ m-wide segments were imaged and EdU⁺Ki67⁻ cells positioned basal to the SVZ counted, followed by the count of all EdU⁺ cells. The ratio of the two counts represented the Q-fraction. One sample each from WT and *Chd8^{+/-del5}* was removed from Q-fraction analysis due to difficulties in selecting the VZ. All immunolabeling was carried out on slide-mounted cryosections (18 μ m) following standard protocols and using primary antibodies directed against Pax6 (ref. 42) (PRB-278P-100; rabbit, 1:100, Covance, Princeton, NJ), Tbr2 (<http://www.abcam.com/TBR2-Eomes-antibody-EPR19012-ab183991.pdf>; ab183991; rabbit, 1:400, Abcam, Cambridge, United Kingdom) or Ki67 (ref. 43) (#12202; rabbit, 1:200, Cell Signaling, Danvers, MA). Alexa Fluor secondary antibodies (488 and 594) were used at 1:200 concentrations (Thermo Fisher Scientific, Waltham, MA). All quantifications of labeled cells were carried out at equivalent anteroposterior positions between genotypes. To determine the dorsoventral position of cortical segments for cell type counts, we measured the cortical ventricle from the corticostriatal boundary to the apex, defined the 50% position and centered at this position a 200- μ m-wide box perpendicular to the ventricle. All imaging was carried out on a Nikon A1 laser scanning confocal microscope.

Lamination assay. P0 or P7 brains were fixed and sectioned as described for “Morphological analysis,” above. Slides were incubated for 24 h at 4 °C in a

blocking solution containing normal donkey serum (5% v/v) diluted in PBS-T (1× phosphate buffered saline and 0.01% (v/v) Triton X-100), rinsed in PBS-T and incubated for 24 h at 4 °C in primary antibody solution containing anti-Ctip2 (ref. 44) (ab18465; Abcam), anti-Tbr1 (ref. 44) (ab31940; Abcam) and anti-Brn2 (ref. 45) (sc-6029; Santa Cruz Biotechnology) antibodies, each diluted 1:500 in PBS-T. These antibodies have been previously used for IHC analysis in brain^{46,47}. The slides were then rinsed in PBS-T and incubated overnight at 4 °C in fluorophore-conjugated secondary antibodies (711-545-152 and 712-165-153; Jackson ImmunoResearch). Slides were rinsed in PBS-T, counterstained for 2 h in DAPI (D1306, Thermo-Fisher), rinsed in PBS-T and coverslip-mounted with Fluoromount-G (SouthernBiotech). Sections were imaged on a Nikon Eclipse E600 upright microscope with a 4× objective lens (Plan Apo; N.A. 0.2), mercury light source, appropriate fluorescent filter sets and NIS Elements software, (v. 4.20; Nikon Instruments). Images were imported into FIJI ImageJ (v. 1.50E⁴⁸) and similar sections from each brain were identified based on anatomical landmarks. Within each genotype, all brains were selected randomly for histological processing without taking morphological criteria into account. All histology was done blind, by investigators who were unaware of group allocation. No data points were excluded. Male and female samples were used. All antibodies used for this study were validated and their use widely reported.

Behavioral testing. Subject mice were housed in a temperature-controlled vivarium maintained on a 12-h light–dark cycle. All procedures were approved by the University of California Davis Institutional Animal Care and Use Committee and were conducted in accordance with the National Institutes of Health Guide for the Care and Use of Laboratory Animals. Efforts were made to minimize pain and distress and the number of animals used. No previous analyses were performed on animals used for behavioral testing. We used mixed genotype home cages with 2–4 animals per cage and used experimenters and video scorer/processors blinded to genotype during testing and analysis. All tests were conducted during the light cycle.

Chd8^{+/-del5} male and female mice and WT littermates, ages 2–4 months, were evaluated in a standard battery of neurobehavioral assays relevant to the core diagnostic and associated symptoms of autism¹⁶. We performed the testing on two independent cohorts of adult *Chd8^{+/-del5}* mice (first cohort: 9 male, 10 female; second cohort: 11 male, 11 female) and WT littermates (first cohort: 11 male, 10 female; second cohort: 11 male, 9 female). One animal in the first cohort died during behavioral testing. This happened during the three-chambered social approach, in the middle of the behavioral battery. Adult *Chd8^{+/-del5}* and matched WT littermates were tested in the following sequence: open field, general health, self-grooming, marble burying, three-chambered social approach, male–female social interactions, novel object recognition and fear conditioning. Testing was performed at the UC Davis MIND Institute Intellectual and Developmental Disabilities Research Center Mouse Behavior Core.

Open field locomotion. General exploratory locomotion in a novel open field environment was assayed as previously described^{49–51}. Open field activity was considered an essential control for effects on physical activity, for example, sedation or hyperactivity^{17,51,52}, which could confound the interpretation of results from the reciprocal interactions, self-grooming, fear conditioning and social approach tasks. The testing room was illuminated at ~40 lx.

Adult general health and neurological reflexes. General health and neurological reflexes were evaluated in adult mice as previously described^{53,54}. General health was assessed on a ranking scale of 0–3 based on fur condition, whisker condition, skin color, and body and limb tone. Body weight and basal temperature were also measured, using a hand held portable scale (Ohaus, Parsippany, NJ) and a mouse thermistor probe with lubricant and gently inserted 2 cm into the rectum, respectively. Righting reflex and any occurrences of physical abnormalities were noted. Neurological reflex tests included trunk curl, wire hanging, forepaw reaching, righting reflex, corneal reflex, whisker twitch, pinnae response, eyeblink response and auditory startle. The reactivity level of each mouse was assessed with tests measuring responsiveness to petting, intensity of a dowel biting response and level of vocalization during handling⁵⁵.

Novel object recognition. The novel object recognition test was conducted in opaque matte white (P95 White, Tap Plastics, Sacramento, CA) open field arenas (40 cm × 60 cm × 23 cm), using methods similar to those previously described^{50,56}. The experiment consisted of three sessions: a 30-min exposure to the open field arena, a 10-min familiarization session and a 5-min recognition

test. On day 1, each subject was habituated to a clean, empty open field arena for 30 min. Twenty-four hours later, each subject was returned to the open field arena for 10 min for the habituation phase. The mouse was then removed from the open field and placed in a clean temporary holding cage for approximately 2 min. Two identical objects were placed in the arena. Each subject was returned to the open field in which it had been habituated and allowed to freely explore for 10 min. After the familiarization session, subjects were returned to their holding cages, which were transferred from the testing room to a nearby holding area. The open field was cleaned with 70% ethanol and let dry. One clean familiar object and one clean novel object were placed in the arena, where the two identical objects had been located during in the familiarization phase. Sixty minutes after the end of the familiarization session, each subject was returned to its open field for a 5 min recognition test, during which time it was allowed to freely explore the familiar object and the novel object. The familiarization session and the recognition test were videotaped and scored with Ethovision XT videotracking software (Version 9.0, Noldus Information Technologies, Leesburg, VA). Object investigation was defined as time spent sniffing the object when the nose was oriented toward the object and the nose–object distance was 2 cm or less. Recognition memory was defined as spending substantially more time sniffing the novel object than the familiar object. Total time spent sniffing both objects was used as a measure of general exploration. Time spent sniffing two identical objects during the familiarization phase confirmed the lack of an innate side bias. Objects used were plastic toys: a small soft plastic orange safety cone and a hard plastic magnetic cone with ribbed sides.

Repetitive self-grooming. Spontaneous repetitive self-grooming behavior was scored as previously described^{17,49}. Each mouse was placed individually into a standard mouse cage (46 cm long × 23.5 cm wide × 20 cm high). Cages were empty to eliminate digging in the bedding, which is a potentially competing behavior. The room was illuminated at ~40 lx. A front-mounted CCTV camera (Security Cameras Direct) was placed ~1 m from the cages to record the sessions. Sessions were videotaped for 20 min. The first 10-min period was habituation and was unscored. Each subject was scored for cumulative time spent grooming all the body regions during the second 10 min of the test session.

Repetitive marble burying. Marble burying and digging in the bedding to cover the marbles was measured as previously described^{49,57–59}. Twenty black glass marbles (15 mm in diameter) were arranged in a symmetrical 4 × 5-cm grid on top of 2–3-cm deep bedding in a clean standard mouse cage (27 × 16.5 × 12.5 cm) with a filter top lid. Each mouse was placed in the center of the cage for a 30-min exploration period, after which the number of marbles buried was tallied by the investigator. ‘Buried’ was defined as greater than 50% covered by bedding⁵⁸. Testing was performed under dim light (~15 lx).

Social approach. Social approach was tested in an automated three-chambered apparatus using methods similar to those previously described^{49,60}. Automated Ethovision XT videotracking software (Version 9.0, Noldus Information Technologies, Leesburg, VA) and modified nonreflective materials for the chambers were employed to maximize throughput. The updated apparatus (40 cm × 60 cm × 23 cm) was a rectangular, three-chambered box made from matte white finished acrylic (P95 White, Tap Plastics, Sacramento, CA). Opaque retractable doors (12 cm × 33 cm) were designed to create optimal entryways between chambers (5 cm × 10 cm), while providing maximal manual division of compartments. Three zones, defined using the EthoVision XT software, detected time in each chamber for each phase of the assay. Zones were defined as the annulus extending 2 cm from each novel object or novel mouse enclosure (inverted wire cup, Galaxy Cup, Kitchen Plus, <https://www.spectrumdiversified.com/whs/products/Galaxy-Pencil-Utility-Cup>). Direction of the head, facing toward the cup enclosure, defined sniff time. A top-mounted infrared-sensitive camera (Ikegami ICD-49, B&H Photo, New York, NY) was positioned directly above every pair of three-chambered units. Infrared lighting (Nightvisionexperts.com) provided uniform, low-level illumination. The subject mouse was first contained in the center chamber for 10 min, then allowed to explore all three empty chambers during a 10 min habituation session, then allowed to explore the three chambers containing a novel object in one side chamber and a novel mouse in the other side chamber. Lack of innate side preference was confirmed during the initial 10 min of habituation to the entire arena. Novel stimulus mice were 129Sv/ImJ, a relatively inactive strain, aged 10–14 weeks, and matched to the subject mice by sex. Number of entries into the side chambers served as a within-task control for levels of general exploratory locomotion.

Male–female social interaction. The male–female reciprocal social interaction test was conducted as previously described^{49,61}. Briefly, each freely moving male subject was paired for 5-min with a freely moving unfamiliar estrous WT female. A closed-circuit television camera (Panasonic, Secaucus, NJ) was positioned at an angle from the Noldus PhenoTyper arena (Noldus, Leesburg, VA) for optimal video quality. An ultrasonic microphone (Avisoft UltraSoundGate condenser microphone capsule CM15; Avisoft Bioacoustics, Berlin, Germany) was mounted 20 cm above the cage. Sampling frequency for the microphone was 250 kHz, and the resolution was 16 bits. The entire apparatus was contained in a sound-attenuating environmental chamber (Lafayette Instruments, Lafayette, IN) under dim LED illumination (~10 lx). Duration of nose-to-nose sniffing, nose-to-anogenital sniffing and following were scored using Noldus Observer 8.0XT event recording software (Noldus, Leesburg, VA) as previously described⁴⁹. Ultrasonic vocalization spectrograms were displayed using Avisoft software and calls were identified manually by a highly trained investigator blinded to genotype.

Fear conditioning. Delay contextual and cued fear conditioning was conducted using an automated fear-conditioning chamber (Med Associates, St Albans, VT, USA) as previously described⁶². The conditioning chamber (32 × 25 × 23 cm³, Med Associates) interfaced with a PC installed with VideoFreeze software (version 1.12.0.0, Med Associates) and enclosed in a sound-attenuating cubicle. Training consisted of a 2-min acclimation period followed by three tone–shock (CS–US) pairings (80-dB tone, duration 30 s; 0.5-mA footshock, duration 1 s; intershock interval, 90 s) and a 2.5-min period during which no stimuli were presented. The environment was well lit (~100 lx) with a stainless steel grid floor and swabbed with vanilla odor cue (prepared from vanilla extract; McCormick; 1:100 dilution). A 5-min test of contextual fear conditioning was performed 24 h after training, in the absence of the tone and footshock but in the presence of 100 lx overhead lighting, vanilla odor and chamber cues identical to those used on the training day. Cued fear conditioning, conducted 48 h after training, was assessed in a novel environment with distinct visual, tactile and olfactory cues. Overhead lighting was turned off. The cued test consisted of a 3-min acclimation period followed by a 3-min presentation of the tone CS and a 90-s exploration period. Cumulative time spent freezing in each condition was quantified by VideoFreeze software (Med Associates).

MRI within brains of the subjects assessed in behavioral assays. *Perfusion.* Mice from the first cohort (*Chd8*^{+/*del5*}; 9 male, 10 female; WT: 8 male, 10 female) that had undergone the behavioral assays were anesthetized with isoflurane (4% to effect) and intracardially perfused with 30 mL of 0.1 M PBS containing 10 U/mL heparin (Sigma) and 2 mM ProHance (a Gadolinium contrast agent) followed by 30 mL of 4% paraformaldehyde (PFA) containing 2 mM ProHance^{63,64}. Mice were perfused and then decapitated, and the skin, lower jaw, ears and the cartilaginous nose tip were removed. The brain and remaining skull structures were incubated in 4% PFA + 2 mM ProHance overnight at 4 °C, then transferred to 0.1 M PBS containing 2 mM ProHance and 0.02% sodium azide for at least 7 d before MRI scanning.

After perfusion, a multichannel 7.0 Tesla MRI scanner (Agilent Inc., Palo Alto, CA) was used to image the brains within their skulls. Sixteen custom-built solenoid coils were used to image the brains in parallel⁶⁵. In order to detect volumetric changes via anatomical imaging, we used the following parameters for the anatomical MRI scans: T2-weighted, 3-D fast spin-echo sequence, with a cylindrical acquisition of *k*-space⁶⁶, a TR of 350 ms and TEs of 12 ms per echo for 6 echoes, field-of-view equal to 20 × 20 × 25 mm³ and matrix size equal to 504 × 504 × 630 mm³. Our parameters output an image with 0.040-mm isotropic voxels. The total imaging time was 14 h.

Diffusion tensor imaging. Diffusion tensor imaging (DTI) was done using a 3D diffusion-weighted fast spin-echo sequence (FSE), with an echo train length of 6. Parameters for the DTI sequence were: TR = 270 ms, first TE = 30 ms and TEs of 10 ms for the remaining five echoes, 1 average. We used a field-of-view (FOV) of 14 × 14 × 25 mm³ and a matrix size of 180 × 180 × 324 mm³, yielding an image with 0.078-mm isotropic voxels. We acquired five *b* = 0 s/mm² images and 30 high *b*-value (*b* = 2,147 s/mm²) images in 30 different directions, using the Jones30 scheme⁶⁷. Total imaging time was ~12 h. After acquisition, the images were analyzed using the FSL software package (FMRIB, Oxford UK), which was used to create fractional anisotropy (FA), mean diffusivity (MD), axial diffusivity (AD) and radial diffusivity (RD) maps for each of the brains used in this study.

Structural MRI registration and analysis. To visualize and compare any changes in the mouse brains the images (or *b* = 0 s/mm² images for DTI) were linearly (6 followed by 12 parameter) and nonlinearly registered together⁶⁸. Registrations were performed with a combination of mni_autoreg tools⁶⁹ and ANTS (advanced normalization tools)^{70,71}. All scans were then resampled with the appropriate transform and averaged to create a population atlas representing the average anatomy of the study sample. Note that the 40- μ m anatomical images and the *b* = 0 s/mm² DTI images were registered separately. The result of the registration was to deform all images into alignment with each other in an unbiased fashion. For the volume measurements, this allowed us to analyze the deformations needed to take each individual mouse's anatomy into this final atlas space, the goal being to model how the deformation fields relate to genotype^{72,73}. The Jacobian determinants of the deformation fields were then calculated as measures of volume at each voxel. For the diffusion measurements, the registration allowed us to analyze the intensity differences of all measures (FA, MD, AD and RD) between genotypes. Significant volume changes and intensity differences could then be calculated by warping a pre-existing classified MRI atlas onto the population atlas, which allowed us to assess the volume or mean diffusion measures (FA, MD, AD and RD) of 159 different segmented structures, encompassing cortical lobes, large white matter structures (i.e., corpus callosum), ventricles, cerebellum, brain stem and olfactory bulbs^{68,74,75}, in all brains. Further, these measurements could be examined on a voxelwise basis to localize the differences found within regions or across the brain. Multiple comparisons in this study were controlled for using the false discovery rate⁷⁶. We reported combined sex results in the main text.

Genomics. Bulk forebrains were microdissected from *Chd8*^{+/*del5*} and matched WT littermates at E12.5, E14.5, E17.5 and P0 and from adults (represented in plots as >P56). Dissection included whole forebrain hemispheres after removing surface tissue and skull for all ages except E12.5, when the anterior portion of the developing head was collected. Dissections were performed blind to genotype. Samples included males and females of each genotype at each stage; exact numbers are reported in **Supplementary Table 2**. Total RNA was isolated using Ambion RNAqueous and assayed using an Agilent BioAnalyzer instrument. Stranded mRNA sequencing libraries were prepared using TruSeq Stranded mRNA kits; 6–12 samples per lane were pooled and sequenced on the Illumina HiSeq platform using a single-end 50-bp (E14.5, E17.5, P0 and adult) or paired-end 100-bp (E12.5) strategy. Each library was quantified and pooled before submission for sequencing. E12.5 samples were sequenced at the UC Berkeley Genomics Sequencing Laboratory; all other samples were sequenced at the UC Davis DNA Technologies Core. Reads from RNA-seq were aligned to the mouse genome (mm9) using STAR (version 2.4.2a)⁷⁷. Aligned reads mapping to genes were counted at the gene level using subreads featureCounts⁷⁸. The mm9 knownGene annotation track and aligned reads were used to generate quality control information using the full RSeQC tool suite⁷⁹. Samples that exhibited strong 3' bias using geneBody_coverage.py or poor exon distribution using read_distribution.py were discarded. Unaligned reads were quality checked by FastQC. BLAST⁸⁰ was used to identify reads that mapped to either the reference or 5-bp and 14-bp deletion at *Chd8* exon 5 to verify genotype and test for deletion allele transcript frequency. We performed quantitative reverse transcription PCR to validate DE and DS analysis using cDNA libraries prepared using the same protocols, with primers reported in **Supplementary Table 4**. Cycle counts were normalized to *Actb* and compared via standard methods as discussed in the methods.

Differential expression analysis and permutation testing. Raw count data for all samples were used as input along with sample information for differential expression analysis using edgeR⁸¹. Genes with at least 10 reads per million in at least two individual samples were included for analysis, resulting in a final set of 11,936 genes for differential testing. Multidimensional scaling analysis indicated that the strongest driver of variance across samples was developmental stage, with no obvious separation between wild-type and *Chd8*^{+/*del5*} samples. Tagwise dispersion estimates were generated, and differential expression analysis was performed with edgeR⁸¹ using a generalized linear model including sex, developmental stage and sequencing run factor-based covariates and using genotype as the variable for testing. Stage-specific differential expression testing was also performed. Normalized expression levels were generated using the edgeR rpk function followed by removing the sequencing batch effect via the limma removeBatchEffect function. Normalized log₂(RPKM) values were used for plotting of

summary heatmaps and of expression data for individual genes. We examined DE results obtained with reduced coverage criteria for gene inclusion, which resulted in identification of DE genes with lower CPM but no major differences in overall findings.

Permutation testing was performed by testing for set inclusion between differentially down- or upregulated genes identified in the full model and annotated gene sets, comparing observed with expected overlap. Observed overlap was calculated as the overlapping genes, whereas the expected overlap distribution was generated via iterative random sampling of the same number of genes as in the annotated gene set, followed by testing for overlap of randomly selected genes with DE genes. Random sampling was repeated 100,000 times, enabling us to estimate the mean and standard deviation of the expected distribution. Based on this distribution, empirical z -scores and P values were calculated for the observed overlap. All analysis was performed in R using custom scripts that are available upon request.

ChIP-seq analysis. Adult mouse forebrain was dissected on ice, cross-linked using formaldehyde and lysed with SDS, and the DNA was sonicated on a Covaris instrument using standard ChIP-seq protocols adapted for mouse tissues⁸². Chromatin immunoprecipitation (ChIP) was performed using antibodies for Chd8 (ab114126; Abcam). This antibody has been used for brain or neuronal Chd8 ChIP-seq in a previous publication¹². DNA libraries of matched input and ChIP samples were prepared using the Nugen Ovation Ultralow Library System V2, indexed for multiplexed runs of four libraries per lane and sequenced on an Illumina HiSeq 4000 instrument using a single-end 50-bp strategy. Resulting reads were filtered to remove artifacts and low-quality sequences, and then mapped to the mouse genome (mm9) using the BWA algorithm⁸³.

BWA call: `bwa aln -t 6 -l 25 mm9 sample.fastq.gz`

We used MACS⁸⁴ to identify significant peaks, disabling model-based peak identification and local significance testing. Peaks were called for each individual ChIP-seq experiment versus matched input control, as well as for merged ChIP and control data using MACS1.4.

MACS call: `macs14 -t chip.bam -control = input.bam -name = chip_output-format = BAM -gsize = mm -tsize = 50 -bw = 300 -mfold = 10,30 -nolambda -nomodel -shiftsize = 150 -p 0.0001`

After peak calling, enriched regions were filtered to remove ENCODE blacklist regions and annotated using custom scripts. As nearly all peaks were at gene promoters, functional annotation was performed on the promoter-bound gene sets using ENRICH⁸⁵. We performed *de novo* motif discovery using RSAT with default parameters⁸⁶. We additionally analyzed available Chd8 ChIP-seq data^{11–13}. For comparison, all datasets were run through the same analysis pipeline and are available as UCSC TrackHubs for upload to the UCSC Genome Browser.

WGCNA. We used the WGCNA package²⁵ in R (version 3.2.3) to construct signed co-expression networks using any gene expressed at an RPKM value of 0.25 or higher in at least one sample. A correlation matrix using the biweight midcorrelation between all genes was computed for all relevant samples. The soft thresholding power was estimated and used to derive an adjacency matrix exhibiting approximate scale-free topology ($R^2 > 0.85$). The adjacency matrix was transformed to a topological overlap matrix (TOM). The matrix 1-TOM was used as the input to calculate co-expression modules using hierarchical clustering. Modules were branches of the hierarchical cluster tree base, using the cutree-Hybrid function in WGCNA⁸⁷, with minimum module size set to 500 genes. Genes with positively correlated expression and high topological overlap were clustered together in these modules. In addition, Pearson's correlation coefficients were used to calculate correlation between sample traits (for example, genotype) and modules. The expression profile of a given module was summarized by the module eigengene, ME. Modules with highly correlated MEs (correlation > 0.80) were merged together. The module connectivity (kME) of each gene was calculated by correlating the gene expression profile with module eigengenes. Four modules were generated using this method and were reordered in descending order by gene set size and named numerically. Genes with no network correlation were placed into the module M.grey. We repeated module generation using only wild-type samples, only *Chd8^{+del5}* samples and with/without adult samples, with largely the same results as for the full sample set, which is consistent with the finding that most DE gene expression changes are far smaller than changes for genes across developmental stages.

Gene Ontology enrichment and protein–protein interaction network analysis. Permutation testing was performed to test for overlap between DE genes and published gene sets. Human Gene Ontology (GO) data was downloaded from Bioconductor (org.Hs.egGO2ALLEGES, org.Hs.eg.db, GO.db). We used the TopGO⁸⁸ program to test for enrichment of GO terms indicating parent:child relationships. For the analysis presented here, we restricted our testing to GO Biological Process annotations and required a minimal node size (number of genes annotated to GO terms) of 20. We used the internal 'weight01' testing framework and the Fisher test, a strategy recommended for gene set analysis that generally accounts for multiple testing comparisons. For GO analysis, we examined down- and upregulated genes separately, repeating the analysis on DE genes from the full model (cutoff of FDR < 0.20) for all genes and by expression module and stage-specific genes sets (cutoff of $P < 0.05$). For all enrichment analysis, the test set of DE genes was compared against the background set of genes expressed in our study based on minimum read-count cutoffs described above. Genes with expected/observed ratios of at least 1.5-fold were considered enriched. Heatmaps showing positive \log_2 (expected/observed) values were plotted for GO terms of interest. Protein–protein interaction enrichment and network generation for module-specific DE gene sets was performed using STRING²⁷, considering only experimentally defined and database interactions. Only module M.1 exhibited a significant enrichment in protein–protein interactions. We compared TopGO enrichment results with goseq⁸⁹, correcting for gene length, and compared STRING protein–protein interaction with DAPPLE⁹⁰, with no substantial differences observed for either methods comparison.

MISO analysis. The Mixture-of-Isoforms (MISO) statistical model³⁰ was used to identify alternative transcript events in our RNA-seq data. For MISO analysis, individual aligned bam files were sorted and merged based on genotype and developmental stage (for example, E17.5 WT and E17.5 *Chd8^{+del5}*). One sample (S159) from the E17.5 *Chd8^{+del5}* group was discarded from analysis because the sample had lower read coverage compared to the other samples and was significantly impacting MISO results across genotype. Analysis was performed using the standard MISO software package fastmiso (<https://github.com/yarden/MISO>). Standard GFF alternate-event annotations for mm9 (version 1) were used. MISO was run to compute PSI scores (miso-run) using standard, unfiltered parameters. Comparisons (compare_miso) were run between either genotype for a specific stage (for example, E17.5 *Chd8^{+del5}* versus E17.5 WT) or pairwise between WT stages (for example, E14.5 WT versus E17.5 WT). Results were filtered (filter_events) based on the following parameters: `-num-total = 100, -num-sum-inc-exc = 10, -delta-psi = 0.1, -bayes-factor = 100`.

Statistical analysis. *General.* No statistical methods were used to predetermine sample sizes, with the exception of behavioral studies, but our other sample sizes are similar to those reported in previous publications^{12,13}. Data collection and analysis were not performed blind to the conditions of the experiments for ChIP-seq, western blots or qRT-PCR. All other data collection and analyses were performed blind. Data collection was randomized across litters for RNA-seq, western blots and histology assays. Aside from behavioral analyses, data distribution was assumed to be normal and not formally tested. A **Supplementary Methods Checklist** is available.

Neuroanatomy, biochemistry and immunostaining. All statistical analyses and plots were generated using GraphPad Prism 7.0a. Two-tailed t -tests were used for all analyses comparing two groups. For comparisons of three or more data sets, one-way ANOVA followed by *post hoc* two-tailed t -tests were used. A minimum of three biological replicates (individual animals) were used for all genotypes and assays. For isoform-specific qPCR, comparisons across stage and genotype were analyzed using two-tailed Welch's t -test and linear regression.

Behavior. Data were analyzed with Statistica software (Tulsa, OK, USA). Plots were generated using GraphPad Prism 7.0a. Sexes were considered separately, with genotype as the fixed factor. Statistical testing was performed using established assay-specific methods, including Student's t -test for single parameter comparisons between genotypes, and one-way or two-way repeated-measures ANOVA were used for comparisons across time points and/or between sexes. All significance levels were set at $P < 0.05$ and all t -tests were two-tailed. Groups sizes indicated were chosen based on past experience and power analyses. Effects of genotype and sex were evaluated using multifactor ANOVA, as previously published^{16,49,50,59,62}. Significant ANOVAs

were followed by Tukey's honest significant difference test. Behavioral analysis passed distribution normality tests, was collected using continuous variables and thus was analyzed via parametric analysis in all assays. For all behavioral analyses, variances were similar between groups and all data points within 2 s.d. of the mean were included in analysis.

Genomic analyses. Samples for RNA-seq were randomly collected across litters and processed blind to genotype. Samples from RNA-seq were removed if they failed to pass quality scoring and coverage criteria. For differential gene expression analysis, differences were considered statistically significant if FDR and *P* values calculated by edgeR were < 0.20 and < 0.05, respectively. For ChIP-seq, peaks were considered significant if *P* values determined by MACS were < 0.0001. For permutation testing, enrichment was considered significant if empirical *z*-scores and *P* values were > 2 and < 0.05, respectively. For differential splicing analysis, individual events were considered significant if the Bayes factor > 100, as calculated by MISO³⁰.

Data availability. The data that support the findings of this study are available from the corresponding author upon reasonable request. DOIs for all published gene sets used in enrichment analysis:

Sanders *et al.*¹⁹: <https://dx.doi.org/10.1016/j.neuron.2015.09.016>;

Pariakshak *et al.*²⁶: <https://dx.doi.org/10.1016/j.cell.2013.10.031>;

Cotney *et al.*¹²: <https://dx.doi.org/10.1038/ncomms7404>;

Willsey *et al.*²¹: <https://dx.doi.org/10.1016/j.cell.2013.10.020>;

Sugathan *et al.*¹¹: <https://dx.doi.org/10.1073/pnas.1405266111>;

Darnell *et al.*²²: <https://dx.doi.org/10.1016/j.cell.2011.06.013>;

Hormozdiari *et al.*²⁰: <https://dx.doi.org/10.1101/gr.178855.114>;

Katayama *et al.*¹³: <https://dx.doi.org/10.1038/nature19357>;

Durak *et al.*¹⁵: <https://dx.doi.org/10.1038/nn.4400>; and

Pariakshak *et al.*²⁴: <https://dx.doi.org/10.1038/nature20612>.

Raw, aligned and gene-count data for RNA-seq and raw, aligned and peak call data for ChIP-seq are available on GEO ([GSE99331](https://www.ncbi.nlm.nih.gov/geo/query/acc.cgi?acc=GSE99331)).

Code availability. All custom scripts and TrackHubs used for data processing and analysis are available in **Supplementary Software** and at the Nord Lab Git Repository (<https://github.com/NordNeurogenomicsLab/>). A custom sample-processing pipeline was used to align raw sequencing samples to mouse genome mm9 using RNA-seq aligner STAR (version 2.4.2a), features assigned via subreads featureCounts (version 1.5.0) to UCSC mm9 genes.gtf and quality checks performed on individual samples using RSeQC (version 2.6.3). Differential expression analysis was done with a custom pipeline in R Studio using functions from edgeR (version 3.10.5) and limma (version 3.24.15). Permutation testing was performed with a custom R script. Co-expression network analysis was performed with a custom pipeline following the standard WGCNA (version 3.2.3) workflow and functions. Gene Ontology analysis was performed with a custom wrapper using standard the TopGO (version 2.20.0) program. ChIP-seq data was aligned to mm9 via BWA (version 0.6.2) and peaks were called via MACS (version 1.4.2). Peaks were then filtered to remove ENCODE blacklist regions and annotated. Comparison of enriched gene sets between RNA and ChIP-seq was performed using Enrichr (<http://amp.pharm.mssm.edu/Enrichr/>). MISO analysis (<https://github.com/yarden/MISO/>) was performed using standard parameters. See above for description and parameters.

39. Mali, P. *et al.* RNA-guided human genome engineering via Cas9. *Science* **339**, 823–826 (2013).
40. Du, C., Ma, X., Meruvu, S., Hugendubler, L. & Mueller, E. The adipogenic transcriptional cofactor ZNF638 interacts with splicing regulators and influences alternative splicing. *J. Lipid Res.* **55**, 1886–1896 (2014).
41. Yoo, S.-W., Motari, M.G. & Schnaar, R.L. Agensis of the corpus callosum in Nogo receptor deficient mice. *J. Comp. Neurol.* **525**, 291–301 (2017).
42. Yeung, J., Ha, T.J., Swanson, D.J. & Goldowitz, D. A novel and multivalent role of Pax6 in cerebellar development. *J. Neurosci.* **36**, 9057–9069 (2016).
43. Nguyen, K.H., Yao, X.-H., Erickson, A.G., Mishra, S. & Nyomba, B.L.G. Glucose intolerance in aging male IGFBP-3 transgenic mice: differential effects of human IGFBP-3 and its mutant IGFBP-3 devoid of IGF binding ability. *Endocrinology* **156**, 462–474 (2015).
44. Galazo, M.J., Emsley, J.G. & Macklis, J.D. Corticothalamic projection neuron development beyond subtype specification: Fog2 and intersectional controls regulate intraclass neuronal diversity. *Neuron* **91**, 90–106 (2016).

45. Espuny-Camacho, I. *et al.* Hallmarks of Alzheimer's disease in stem-cell-derived human neurons transplanted into mouse brain. *Neuron* **93**, 1066–1081.e8 (2017).
46. Huang, Z., Yu, Y., Shimoda, Y., Watanabe, K. & Liu, Y. Loss of neural recognition molecule NB-3 delays the normal projection and terminal branching of developing corticospinal tract axons in the mouse. *J. Comp. Neurol.* **520**, 1227–1245 (2012).
47. Lloyd-Burton, S. & Roskams, A.J. SPARC-like 1 (SC1) is a diversely expressed and developmentally regulated matricellular protein that does not compensate for the absence of SPARC in the CNS. *J. Comp. Neurol.* **520**, 2575–2590 (2012).
48. Schindelin, J. *et al.* Fiji: an open-source platform for biological-image analysis. *Nat. Methods* **9**, 676–682 (2012).
49. Silverman, J.L. *et al.* GABAB receptor agonist R-baclofen reverses social deficits and reduces repetitive behavior in two mouse models of autism. *Neuropsychopharmacology* **40**, 2228–2239 (2015).
50. Flannery, B.M. *et al.* Behavioral assessment of NIH Swiss mice acutely intoxicated with tetramethylenedisulfotetramine. *Neurotoxicol. Teratol.* **47**, 36–45 (2015).
51. Silverman, J.L. *et al.* Negative allosteric modulation of the mGluR5 receptor reduces repetitive behaviors and rescues social deficits in mouse models of autism. *Sci. Transl. Med.* **4**, 131ra51 (2012).
52. Silverman, J.L. *et al.* Low stress reactivity and neuroendocrine factors in the BTBR T+tf/J mouse model of autism. *Neuroscience* **171**, 1197–1208 (2010).
53. Wöhr, M. & Scattoni, M.L. Behavioural methods used in rodent models of autism spectrum disorders: current standards and new developments. *Behav. Brain Res.* **251**, 5–17 (2013).
54. Chadman, K.K. *et al.* Minimal aberrant behavioral phenotypes of neuroligin-3 R451C knockin mice. *Autism Res.* **1**, 147–158 (2008).
55. Rogers, D.C. *et al.* Behavioral and functional analysis of mouse phenotype: SHIRPA, a proposed protocol for comprehensive phenotype assessment. *Mamm. Genome* **8**, 711–713 (1997).
56. Yang, M., Lewis, F.C., Sarvi, M.S., Foley, G.M. & Crawley, J.N. 16p11.2 Deletion mice display cognitive deficits in touchscreen learning and novelty recognition tasks. *Learn Mem.* **22**, 622–632 (2015).
57. Thomas, A.M., Bui, N., Perkins, J.R., Yuva-Paylor, L.A. & Paylor, R. Group I metabotropic glutamate receptor antagonists alter select behaviors in a mouse model for fragile X syndrome. *Psychopharmacology (Berl.)* **219**, 47–58 (2012).
58. Thomas, A. *et al.* Marble burying reflects a repetitive and perseverative behavior more than novelty-induced anxiety. *Psychopharmacology (Berl.)* **204**, 361–373 (2009).
59. Henderson, C. *et al.* Reversal of disease-related pathologies in the fragile X mouse model by selective activation of GABAB receptors with arbaclofen. *Sci. Transl. Med.* **4**, 152ra128 (2012).
60. Yang, M., Silverman, J.L. & Crawley, J.N. Automated three-chambered social approach task for mice. in *Current Protocols in Neuroscience* (eds. Gerfen, C.R., Holmes, A., Sibley, D., Skolnick, P. & Wray, S.) Chapter 8, Unit 8.26–8.26.16 (Wiley, 2011).
61. Scattoni, M.L., Ricceri, L. & Crawley, J.N. Unusual repertoire of vocalizations in adult BTBR T+tf/J mice during three types of social encounters. *Genes Brain Behav.* **10**, 44–56 (2011).
62. Bales, K.L. *et al.* Long-term exposure to intranasal oxytocin in a mouse autism model. *Transl. Psychiatry* **4**, e480 (2014).
63. Skrzypiec-Spring, M., Grotthaus, B., Szelag, A. & Schulz, R. Isolated heart perfusion according to Langendorff—still viable in the new millennium. *J. Pharmacol. Toxicol. Methods* **55**, 113–126 (2007).
64. Cahill, L.S. *et al.* Preparation of fixed mouse brains for MRI. *Neuroimage* **60**, 933–939 (2012).
65. Bock, N.A. *et al.* In vivo magnetic resonance imaging and semiautomated image analysis extend the brain phenotype for *cdf/cdf* mice. *J. Neurosci.* **26**, 4455–4459 (2006).
66. Nieman, B.J. *et al.* Fast spin-echo for multiple mouse magnetic resonance phenotyping. *Magn. Reson. Med.* **54**, 532–537 (2005).
67. Jones, D.K., Horsfield, M.A. & Simmons, A. Optimal strategies for measuring diffusion in anisotropic systems by magnetic resonance imaging. *Magn. Reson. Med.* **42**, 515–525 (1999).
68. Dorr, A.E., Lerch, J.P., Spring, S., Kabani, N. & Henkelman, R.M. High resolution three-dimensional brain atlas using an average magnetic resonance image of 40 adult C57Bl/6J mice. *Neuroimage* **42**, 60–69 (2008).
69. Collins, D.L., Neelin, P., Peters, T.M. & Evans, A.C. Automatic 3D intersubject registration of MR volumetric data in standardized Talairach space. *J. Comput. Assist. Tomogr.* **18**, 192–205 (1994).
70. Avants, B.B. *et al.* A reproducible evaluation of ANTs similarity metric performance in brain image registration. *Neuroimage* **54**, 2033–2044 (2011).
71. Avants, B.B., Epstein, C.L., Grossman, M. & Gee, J.C. Symmetric diffeomorphic image registration with cross-correlation: evaluating automated labeling of elderly and neurodegenerative brain. *Med. Image Anal.* **12**, 26–41 (2008).
72. Lerch, J.P. *et al.* Cortical thickness measured from MRI in the YAC128 mouse model of Huntington's disease. *Neuroimage* **41**, 243–251 (2008).
73. Nieman, B.J., Flenniken, A.M., Adamson, S.L., Henkelman, R.M. & Sled, J.G. Anatomical phenotyping in the brain and skull of a mutant mouse by magnetic resonance imaging and computed tomography. *Physiol. Genomics* **24**, 154–162 (2006).
74. Steadman, P.E. *et al.* Genetic effects on cerebellar structure across mouse models of autism using a magnetic resonance imaging atlas. *Autism Res.* **7**, 124–137 (2014).
75. Ullmann, J.F.P., Janke, A.L., Reutens, D. & Watson, C. Development of MRI-based atlases of non-human brains. *J. Comp. Neurol.* **523**, 391–405 (2015).

76. Genovese, C.R., Lazar, N.A. & Nichols, T. Thresholding of statistical maps in functional neuroimaging using the false discovery rate. *Neuroimage* **15**, 870–878 (2002).
77. Dobin, A. *et al.* STAR: ultrafast universal RNA-seq aligner. *Bioinformatics* **29**, 15–21 (2013).
78. Liao, Y., Smyth, G.K. & Shi, W. featureCounts: an efficient general purpose program for assigning sequence reads to genomic features. *Bioinformatics* **30**, 923–930 (2014).
79. Wang, L., Wang, S. & Li, W. RSeQC: quality control of RNA-seq experiments. *Bioinformatics* **28**, 2184–2185 (2012).
80. Altschul, S.F., Gish, W., Miller, W., Myers, E.W. & Lipman, D.J. Basic local alignment search tool. *J. Mol. Biol.* **215**, 403–410 (1990).
81. Robinson, M.D., McCarthy, D.J. & Smyth, G.K. edgeR: a Bioconductor package for differential expression analysis of digital gene expression data. *Bioinformatics* **26**, 139–140 (2010).
82. Nord, A.S. *et al.* Rapid and pervasive changes in genome-wide enhancer usage during mammalian development. *Cell* **155**, 1521–1531 (2013).
83. Li, H. & Durbin, R. Fast and accurate short read alignment with Burrows-Wheeler transform. *Bioinformatics* **25**, 1754–1760 (2009).
84. Feng, J., Liu, T. & Zhang, Y. Using MACS to identify peaks from ChIP-seq data. in *Current Protocols in Bioinformatics* (eds. Bateman, A., Draghici, S., Khurana, E., Orchard, S. & Pearson, W.R.) Chapter 2, Unit 2.14 (Wiley, 2011).
85. Chen, E.Y. *et al.* Enrichr: interactive and collaborative HTML5 gene list enrichment analysis tool. *BMC Bioinformatics* **14**, 128 (2013).
86. Medina-Rivera, A. *et al.* RSAT 2015: regulatory sequence analysis tools. *Nucleic Acids Res.* **43**, W50–6 (2015).
87. Zhang, B. & Horvath, S. A general framework for weighted gene co-expression network analysis. *Stat. Appl. Genet. Mol. Biol.* **4**, e17 (2005).
88. Van Laere, S. *et al.* Distinct molecular phenotype of inflammatory breast cancer compared to non-inflammatory breast cancer using Affymetrix-based genome-wide gene-expression analysis. *Br. J. Cancer* **97**, 1165–1174 (2007).
89. Young, M.D., Wakefield, M.J., Smyth, G.K. & Oshlack, A. Gene ontology analysis for RNA-seq: accounting for selection bias. *Genome Biol.* **11**, R14 (2010).
90. Rossin, E.J. *et al.* Proteins encoded in genomic regions associated with immune-mediated disease physically interact and suggest underlying biology. *PLoS Genet.* **7**, e1001273 (2011).

Corresponding Author: Nord

Manuscript Number: NN-A57672

Manuscript Type: Article

Main Figures: 8

Supplementary Figures: 7

Supplementary Tables: 8

Supplementary Videos: 0

Reporting Checklist for Nature Neuroscience

This checklist is used to ensure good reporting standards and to improve the reproducibility of published results. For more information, please read [Reporting Life Sciences Research](#).

Please note that in the event of publication, it is mandatory that authors include all relevant methodological and statistical information in the manuscript.

▶ Statistics reporting, by figure

- Please specify the following information for each panel reporting quantitative data, and where each item is reported (section, e.g. Results, & paragraph number).
- Each figure legend should ideally contain an exact sample size (n) for each experimental group/condition, where n is an exact number and not a range, a clear definition of how n is defined (for example x cells from x slices from x animals from x litters, collected over x days), a description of the statistical test used, the results of the tests, any descriptive statistics and clearly defined error bars if applicable.
- For any experiments using custom statistics, please indicate the test used and stats obtained for each experiment.
- Each figure legend should include a statement of how many times the experiment shown was replicated in the lab; the details of sample collection should be sufficiently clear so that the replicability of the experiment is obvious to the reader.
- For experiments reported in the text but not in the figures, please use the paragraph number instead of the figure number.

Note: Mean and standard deviation are not appropriate on small samples, and plotting independent data points is usually more informative. When technical replicates are reported, error and significance measures reflect the experimental variability and not the variability of the biological process; it is misleading not to state this clearly.

	TEST USED		n			DESCRIPTIVE STATS (AVERAGE, VARIANCE)		P VALUE		DEGREES OF FREEDOM & F/t/z/R/ETC VALUE		
	FIGURE NUMBER	WHICH TEST?	SECTION & PARAGRAPH #	EXACT VALUE	DEFINED?	SECTION & PARAGRAPH #	REPORTED?	SECTION & PARAGRAPH #	EXACT VALUE	SECTION & PARAGRAPH #	VALUE	SECTION & PARAGRAPH #
example	1a	one-way ANOVA	Fig. legend	9, 9, 10, 15	mice from at least 3 litters/group	Methods para 8	error bars are mean +/- SEM	Fig. legend	p = 0.044	Fig. legend	F(3, 36) = 2.97	Fig. legend
example	results, para 6	unpaired t-test	Results para 6	15	slices from 10 mice	Results para 6	error bars are mean +/- SEM	Results para 6	p = 0.0006	Results para 6	t(28) = 2.808	Results para 6
+ - +	1A-1C	NA										

		TEST USED		n			DESCRIPTIVE STATS (AVERAGE, VARIANCE)		P VALUE		DEGREES OF FREEDOM & F/t/z/R/ETC VALUE	
FIGURE NUMBER	WHICH TEST?	SECTION & PARAGRAPH #	EXACT VALUE	DEFINED?	SECTION & PARAGRAPH #	REPORTED?	SECTION & PARAGRAPH #	EXACT VALUE	SECTION & PARAGRAPH #	VALUE	SECTION & PARAGRAPH #	
+ -	1D	Unpaired t-test	Results para 2	17	WT=9, HT=8	Fig legend	Error bars are mean +/- SEM	Fig legend	p=0.0076	Fig legend	t=4.037 df=15	
+ -	1E	Unpaired t-test	Results para 2	12, 18	e14.5: WT=6, HT=6 P0: WT=9, HT=9	Fig legend	Error bars are mean +/- SEM	Fig legend	e14.5: p=0.02 P0: p=0.0089	Fig legend	e14.5: t=2.765, df=10 P0: t=2.977, df=16	
+ -	1F	One way ANOVA, post hoc t-test	Results para 3	10, 20	WT-M=4, WT-F=6, HT-F=10, HT-M=10	Fig legend	Error bars are mean +/- SEM	Fig legend	ANOVA p<0.0001 M: p<0.0001 F: p<0.0001	Fig legend	Male: t=6.317, df=14 Female: t=6.126, df=12 Anova: R2=0.7764, F(3,26)=1.946	
+ -	1G	NA	Results para 3									
+ -	1H	Unpaired t-test	Results para 3	8	WT=4 (2 M, 2 F), HT=4 (2 M, 2 F)	Fig legend	Error bars are mean +/- SEM	Fig legend	Area: p=0.0328 30% Thickness: p=0.224 70% Thickness: p=0.268 Length: p=0.0026	Fig legend	Area: t=2.76, df=6 30% Thickness: t=1.221, df=6 70% Thickness: t=1.355, df=6 Length: t=4.944, df=6	
+ -	2A	Unpaired t-test	Results para 4	39	WT=20, HT=19 littermates	Results para 4	Error bars are mean +/- SEM	Fig legend	p=0.0019	Fig legend	t(1, 37)=3.3492	Fig legend
+ -	2B	Unpaired t-test	Results para 4	39	WT=20, HT=19 littermates	Results para 4	Error bars are mean +/- SEM	Fig legend	p=0.0104	Fig legend	t(1, 37)=2.7064	Fig legend
+ -	2C	Repeated measures ANOVA	Results para 4	39	WT=20, HT=19 littermates	Results para 4	Error bars are mean +/- SEM	Fig legend	WT p=0.0031 HT p=0.0867	Fig legend	WT F(1, 19)=11.5030, HT F(1, 18)=3.2825	Fig legend
+ -	2D	Repeated measures ANOVA & Two factor ANOVA	Results para 5	39	WT=20, HT=19 littermates	Results para 4	Error bars are mean +/- SEM	Fig legend	Repeated measures: WT p=0.0007 HT p=0.0059 Two factor: p=0.149	Fig legend, Results para 5	WT F(1, 19)=16.31 HT F(1, 18)=9.744 Two factor: F(1, 37)=2.16	Fig legend, Results para 5
+ -	2E	Repeated measures ANOVA & Two factor ANOVA	Results para 5	37	WT=19, HT=18 littermates	Results para 4	Error bars are mean +/- SEM	Fig legend	WT p=0.0164 HT p=0.0023 Two factor: p=0.7555	Fig legend, Results para 5	WT F(1, 18)=7.00369, HT F(1, 17)=12.8051, Two factor: F(1, 35)=0.0985	Fig legend, results para 5
+ -	2F	One-way ANOVA	Results para 5	39	WT=20, HT=19 littermates	Results para 4	Error bars are mean +/- SEM	Fig legend	p=0.73 Habituation: p=0.584	Fig legend	F(1, 37)=0.11 Habituation: F(1, 37)=0.30	Fig legend, results para 5
+ -	2G	Unpaired t-test	Results para 5	19	WT=10, HT=9 littermates	Results para 4	Error bars are mean +/- SEM	Fig legend	p=0.3599	Fig legend	t(1, 17)=0.9409	Fig legend
+ -	2H	Unpaired t-test	Results para 5	19	WT=10, HT=9 littermates	Results para 4	Error bars are mean +/- SEM	Fig legend	p=0.5705	Fig legend	t(1, 17)=0.5785	Fig legend
+ -	2I	Unpaired t-test	Results para 5	19	WT=10, HT=9 littermates	Results para 4	Error bars are mean +/- SEM	Fig legend	p=0.8722	Fig legend	t(1, 17)=0.1634	Fig legend

+ -	2J	Unpaired t-test	Results para 5	40	WT=20, HT=20 littermates (Sex differences: WT=19, HT=19)	Results para 4	Error bars are mean +/- SEM	Fig legend	p=0.3978 Sex diff: p = 0.619	Fig legend, results para 5	t(1, 38)=0.8552 Sex diff: t(1, 36) = -0.504	Fig legend, results para 5
+ -	2K	Unpaired t-test	Results para 5	40	WT=20, HT=20 littermates	Results para 4	Error bars are mean +/- SEM	Fig legend	p=0.3165 p=0.1449	Fig legend	t(1, 38)=1.0151 Sex diff: t(1, 38)=1.4883	Fig legend, results para 5
+ -	2L	Unpaired t-test	Results para 5	40	WT=20, HT=20 littermates	Results para 4	Error bars are mean +/- SEM	Fig legend	p=0.2455	Fig legend	t(1, 38)=1.1795	Fig legend
+ -	3A	Unpaired t-test	Results para 6	37	18 HT (8 m, 10 f), 19 WT (9 m, 10 f)	Methods	All relevant stats reported	Table S1	Cortex: p<0.0001, Amygdala: p<0.0001, Hippocampus: p<0.0001	Fig legend	Cortex: t=4.511, df=35 Amygdala: t=4.57, df=35 Hippocampus: t=4.646, df=35	
+ -	3B	Unpaired t-test	Results para 6	37	18 HT (8 m, 10 f), 19 WT (9 m, 10 f)	Methods	Error bars are mean +/- SEM	Table S1	Cortex: p=0.0147, Amygdala: p=0.0010, Hippocampus: p=0.0004	Fig legend, Table S1	Cortex: t=2.566 df=35 Amygdala: t=3.599 df=35 Hippocampus: t=3.896 df=35	
+ -	3C	Voxel-wise FDR	Results para 6	37	18 HT (8 m, 10 f), 19 WT (9 m, 10 f)	Methods	All relevant stats reported	Table S1	All relevant stats reported	Table S1	All relevant stats reported	Table S1
+ -	3E	Generalized linear regression model	Results para 7	37	18 HT (8 m, 10 f), 19 WT (9 m, 10 f)	Methods	% Time (exact value) vs. Volume	Table S1	Cortex: R2=0.1855, Hippocampus: R2=0.148, Amygdala R2=0.1352	Fig legend, Table S1	Cortex: F-stat=33.6, FDR<0.1% Hippocampus: F-stat=29.0, FDR<0.1%, Amygdala: F-stat=38.6, FDR<0.1%	Results para 7, Table S1
+ -	3D	FDR-corrected Regional Analysis	Results para 6	37	18 HT (8 m, 10 f), 19 WT (9 m, 10 f)	Methods	Full statistical results reported	Table S1	Full statistical results reported	Table S1	Full statistical results reported	Table S1
+ -	4A	NA	Results para 8									
+ -	4B	Generalized linear regression model (EdgeR)	Results para 9	44	WT=18, HT=26 littermates	Tables S2	Full statistical results reported	Table S3	Full statistical results reported	Table S4	Full statistical results reported	Table S3
+ -	4C	Generalized linear regression model (EdgeR)	Results para 9	44	WT=18, HT=26 littermates	Table S2	Error bars are mean +/- SEM	Table S3	p=2.2E-27 FDR=3.18E-23	Table S4	Full statistical results reported	Table S3
+ -	4D	Generalized linear regression model (EdgeR)	Results para 9	44	WT=18, HT=26 littermates	Table S2	Error bars are mean +/- SEM	Table S3	Kdm5b: FDR=1.4E-02, Bcl11a: FDR=2.5E-02, Hnrnpa2b1: FDR=1.9E-02	Table S4	Full statistical results reported	Table S3
+ -	4E	Unpaired t-test	Results para 9	10, 10	Hnrnpa2b1: qPCR - WT=6, HT=4 WB - WT=5, HT=5	Fig legend	Error bars are mean +/- SEM	Fig legend	qPCR: p=0.0248, WB: p=0.0055	Fig legend	qPCR: t=2.691, df=8 WB: t=3.765, df=8	
+ -	4F	ChIP-seq peak calling	Results para 10	44	WT=18, HT=26 littermates	Table S2	Relevant stats reported	Table S3	MACS p<0.0001	Methods & Table S4	Relevant stats reported	Table S3

+ -	4G	Enrichr GO gene set enrichment analysis	Results para 10	44	WT=18, HT=26 littermates	Table S2	Relevant stats reported in table	Fig	mRNA processing: p=6.62E-14, 1.37E-12, Chromatin mod: p=8.56E-11, 1.57E-12; Reg of Cell Cycle: p=0.0317, 0.0021	Fig	Relevant stats reported in table	Fig, Table S5
+ -	4H	Permutation test: gene set compared for test and random sample (100k) set against DE genes	Results para 11	44	WT=18, HT=26 littermates	Table S2	Relevant stats reported	Table S4	Permutation p=2.8E-10	Results para	Relevant stats reported	Table S7
+ -	4I	Permutation test	Results para 11	44	WT=18, HT=26 littermates	Table S2	Relevant stats reported	Table S3	Z-scores shown top-to-bottom: 8.2, 6.3, 6.8, 4.8, 2.0, 0.3, 2.5 FMRP p=0.04 DE-up.ASD p=0.012	Fig		
+ -	4J	Permutation test	Results para 10/12	44	WT=18, HT=26 littermates	Table S2	Relevant stats reported	Table S3	Z-scores shown top-to-bottom: 10.2, 14.2, 4.8, 3.4, 15.0, 3.7, 3.2, 10.6	Fig		
+ -	5A	Generalized linear regression model	Results para 13	44	WT=18, HT=26 littermates	Table S2	Relevant stats reported	Table S3				
+ -	5B	WGCNA	Results para 13	44	WT=18, HT=26 littermates	Table S2	Relevant stats reported	Table S7				
+ -	5C	Generalized linear regression model	Results para 13	44	WT=18, HT=26 littermates	Table S2	Mean +/- 1 SD	Table S3	All relevant stats reported	Table S4	All relevant stats reported	Table S3
+ -	5D	GO Enrichment (TopGO)	Results para 13	44	WT=18, HT=26 littermates	Table S2	Relevant stats reported	Table S7	All relevant stats reported	Table S7	All relevant stats reported	Table S7
+ -	5E	Permutation test	Results para 13	44	WT=18, HT=26 littermates	Table S2	Relevant stats reported	Table S7	Z-scores: M1: 10.2, NA M2: NA, 5.0 M3: 11.3, NA M4: NA, 9.7 Mgrey: NA, 10.9	Fig	Relevant stats reported	Table S7

+ -	5F	Permutation test	Results para 13	44	WT=18, HT=26 littermates	Table S2	Relevant stats reported	Table S7	Z-scores top-to-bottom, by module: Katayama up: 12.60, 5.23, 4.85, 6.88, 3.55 Katayama down: 6.80, 7.22, 2.51, 2.92, 0.33 Durak up: 1.27, 3.39, 1.47, 4.24 Durak down: 10.1, 5.26, 3.58, 5.24 Chd8 up: 1.01, 0.96 Chd8 down: 10.2, 0.50, 0.77, 0.27 Sanders down: 5.81, 2.22, 1.06, 2.47 Willsey down: 5.13, 1.26, 3.95, 2.30 Hormozdiari down: 5.8, 1.68, 0.81 Darnell up: 0.88 Darnell down: 4.30, 0.22, 0.73, 0.31	Fig	Relevant stats reported	Fig, Table S7
+ -	5G	Permutation test	Results para 13	44	WT=18, HT=26 littermates	Table S2	Relevant stats reported	Table S7	Z-scores top-to-bottom, by module: M2 down: 11.51, 2.59, 7.35, 4.62 M3 up: 2.05, 0.79 M3 down: 9.33, 0.11, 1.71 M13 up: 9.24, 1.30 M16 up: 3.07, 1.51 M16 down: 2.77 M17 up: 1.59 M17 down: 2.58 M9 up: 1.06, 7.55, 3.77 M19 up: 3.90, 0.52	Fig	Relevant stats reported	Table S7
+ -	6A	Generalized linear regression model & Permutation test	Results para 14	44	WT=18, HT=26 littermates	Table S2	Mean +/- 1 SD	Table S3	permutation p $p=8.8e-26$	Table S7	All relevant stats reported	Table S7
+ -	6B	Generalized linear regression model	Results para 14	44	WT=18, HT=26 littermates	Table S2	Mean Effect Size in Pseudo-counts	Fig	All relevant stats reported	Table S3	All relevant stats reported	Table S3

+ -	6C	STRING: protein-protein interactions (observed vs expected)	Results para 14	44	WT=18, HT=26 littermates	Table S2	NA	NA	Reported as calculated using STRING: $p < 0.0001$	Results para 14	All relevant stats reported	Results para 14
+ -	6D	NA	Results para 14									
+ -	6E	Unpaired type 2 t-test	Results para 15	8	WT=4, HT=4	Fig legend	Error bars are mean +/- SEM	Fig legend	$p = 0.0388$	Fig legend	$t = 2.636$ $df = 6$	
+ -	7A	NA	Results para 16	8	WT=4, HT=4	Fig legend	NA		NA			
+ -	7B	NA	Results para 16	8	WT=4, HT=4	Fig legend	NA		NA			
+ -	7C	NA	Results para 16	8	WT=4, HT=4	Fig legend	NA		NA			
+ -	7D	NA	Results para 16	8	WT=3, HT=3	Fig legend	NA		NA			
+ -	7E	Unpaired t-test	Results para 16	8	WT=4, HT=4	Fig legend	Error bars are mean +/- SEM	Fig legend	$p = 0.0165$	Fig legend	$t = 3.294$, $df = 6$	
+ -	7F	Unpaired t-test	Results para 16	8	WT=4, HT=4	Fig legend	Error bars are mean +/- SEM	Fig legend	$p = 0.0032$	Fig legend	$t = 4.733$, $df = 6$	
+ -	7G	Unpaired t-test	Results para 16	8	WT=4, HT=4	Fig legend	Error bars are mean +/- SEM	Fig legend	$p = 0.0086$	Fig legend	$t = 3.84$, $df = 6$	
+ -	7H	Unpaired t-test	Results para 16	6	WT=3, HT=3	Fig legend	Error bars are mean +/- SEM	Fig legend	$p = 0.0057$	Fig legend	$t = 5.406$, $df = 4$	
+ -	8A	Generalized linear regression model	Results para 17	44	WT=18, HT=26 littermates	Table S2	Mean +/- 1 SD	Fig legend	FDR: Srsf7 = $5e-02$ Hnnpa1 = $3.6-03$ Dhx9 = $7e-02$ Upf3b = $6.9e-05$	Table S3, Fig	All relevant stats reported	Table S3
+ -	8B	Reactome gene set enrichment	Results para 17	1130	1130 DE (FDR < 0.20) genes identified in reactome DB	Table S2	All relevant stats reported	Table S6	All relevant stats reported	Table S6	All relevant stats reported	Table S6
+ -	8C	MISO statistical model	Results para 18	9	e17.5: WT=2, HT=7 (591 total events on bar plot, 395 dark grey)	Table S8	All relevant stats reported	Table S8	BF>100, All relevant stats reported	Table S8	All relevant stats reported	Table S8
+ -	8D	MISO statistical model	Results para 18	9, 9	e17.5: WT=2, HT=7 e14.5: WT=3, HT=6	Table S8	All relevant stats reported	Table S8	BF>100, All relevant stats reported	Table S8	All relevant stats reported	Table S8
+ -	8E	NA										
+ -	8F	Welch's t-test, Generalized linear regression	Results para 29	41	e12.5=7 e14.5=9 e17.5-WT=7, e17.5-HT=7 P0=11	Fig legend	Error bars are mean +/- SEM	Fig legend	e14.5-e17.5: $p = 0.001$ e17.5-e17.5: $p = 0.03$ Dev time: $p = 4.53E-14$ Dev time: $R^2 = 0.77$	Fig legend	e14.5-e17.5: $t = 4.1708$, $df = 13.622$ e17.5-e17.5: $t = -2.4352$, $df = 11.632$	

+ -	S1A	One way ANOVA, unpaired post hoc t-test	Results para 2	10	WT=3 (280), WT=4 (110), HT-5bp=3, HT-14bp=3	Fig legend	Error bars are mean +/- SEM	Fig legend	280 kDa ANOVA: $p=0.0118$ 110 kDa ANOVA: $p=0.1676$ 280 kDa: 5bp $p=0.0319$; 14bp $p=0.0328$ 110 kDa: 5bp $p=0.1086$, 14bp $p=0.4509$	Fig legend	280 kDa ANOVA: $F=10.19$, $R^2=0.7726$ 110 kDa ANOVA: $F=2.33$, $R^2=0.3997$ 280 5bp $t=3.233$, $df=4$ 280 14bp $t=3.203$, $df=4$ 110 5bp $t=1.951$, $df=5$; 14bp $t=0.8174$, $df=5$	
+ -	S1B	Unpaired t-test	Results para 2	18	WT=9, HT=9	Fig legend	Error bars are mean +/- SEM	Fig legend	280 kDa: $p=0.0089$ 110 kDa: $p=0.001$	Fig legend	280 kDa: $t=2.977$, $df=16$ 110 kDa: $t=4.022$, $df=16$	
+ -	S1C	Unpaired t-test	Results para 2	12	WT=6, HT=6	Fig legend	Error bars are mean +/- SEM	Fig legend	280 kDa: $p=0.9903$ 110 kDa: $p=0.02$	Fig legend	280 kDa: $t=2.765$, $df=10$ 110 kDa: $t=0.01248$, $df=10$	
+ -	S2A	Unpaired t-test	Results para 4	42	WT=20, HT=22	Fig legend	Error bars are mean +/- SEM	Fig legend	$p=0.1046$	Fig legend	$t(1, 40)=1.6607$	Fig legend
+ -	S2B	Unpaired t-test	Results para 4	42	WT=20, HT=22	Fig legend	Error bars are mean +/- SEM	Fig legend	$p=0.0571$	Fig legend	$t(1, 40)=1.9593$	Fig legend
+ -	S2C	Repeated measures ANOVA	Results para 4	41	WT=21, HT=20 littermates	Fig legend	Error bars are mean +/- SEM	Fig legend	WT $p=0.0453$ HT $p=0.3846$	Fig legend	WT $F(1, 20)=4.5583$, HT $F(1, 19)=0.7921$	Fig legend
+ -	S2D	Repeated measures ANOVA	Results para 4	42	WT=21, HT=21	Fig legend	Error bars are mean +/- SEM	Fig legend	WT $p=0.0042$ HT $p=0.0008$	Fig legend	WT $F(1, 20)=10.438$ HT $F(1, 20)=15.470$	Fig legend
+ -	S2E	Repeated measures ANOVA	Results para 4	42	WT=21, HT=21	Fig legend	Error bars are mean +/- SEM	Fig legend	WT $p=0.0002$ HT $p=0.00002$	Fig legend	WT $F(1, 20)=20.3750$ HT $F(1, 20)=30.3946$	Fig legend
+ -	S2F	One-way ANOVA	Results para 4	42	WT=21, HT=21	Fig legend	Error bars are mean +/- SEM	Fig legend	$p=0.583$	Fig legend	$F(1, 40)=0.307$	Fig legend
+ -	S2G	Unpaired t-test	Results para 4	22	WT=11, HT=11	Fig legend	Error bars are mean +/- SEM	Fig legend	$p=0.8807$	Fig legend	$t(1, 20) = 0.1520$	Fig legend
+ -	S2H	Unpaired t-test	Results para 4	22	WT=11, HT=11	Fig legend	Error bars are mean +/- SEM	Fig legend	$p=0.8057$	Fig legend	$t(1, 20)=0.2492$	Fig legend
+ -	S2I	Unpaired t-test	Results para 4	22	WT=11, HT=11	Fig legend	Error bars are mean +/- SEM	Fig legend	$p=0.1167$	Fig legend	$t(1, 20)=1.6396$	Fig legend
+ -	S2J	Unpaired t-test	Results para 4	22	WT=11, HT=11	Fig legend	Error bars are mean +/- SEM	Fig legend	$p=0.4914$	Fig legend	$t(1, 20)=0.7010$	Fig legend
+ -	S2K	Unpaired t-test	Results para 4	44	WT=22, HT=22	Fig legend	Error bars are mean +/- SEM	Fig legend	$p=0.8047$	Fig legend	$t(1, 40)=0.2489$	Fig legend
+ -	S2L	Unpaired t-test	Results para 4	44	WT=22, HT=22	Fig legend	Error bars are mean +/- SEM	Fig legend	$p=0.3328$	Fig legend	$t(1, 40)=0.9799$	Fig legend
+ -	S3	Voxel-wise FDR	Results para 6	37	18 HT (8 m, 10 f), 19 WT (9 m, 10 f)	Table S1	Effect size	Table S1	All relevant stats (FDR, p) reported	Table S1	All relevant stats reported	Table S1
+ -	S4A	Unpaired t-test	Results para 9	13	WT=6, HT=7	Fig legend	Error bars are mean +/- SEM	Fig legend	$p=0.5221$	Fig legend	$t=0.6612$, $df=11$	
+ -	S4B	Unpaired t-test	Results para 9	8	WT=4, HT=4	Fig legend	Error bars are mean +/- SEM	Fig legend	$p=0.5888$	Fig legend	$t=0.5663$, $df=7$	
+ -	S4C	Unpaired t-test	Results para 9	11	WT=6, HT=5	Fig legend	Error bars are mean +/- SEM	Fig legend	$p=0.0851$	Fig legend	$t=1.935$, $df=9$	
+ -	S4D	Unpaired t-test	Results para 9	11	WT=6, HT=5	Fig legend	Error bars are mean +/- SEM	Fig legend	$p=0.0383$	Fig legend	$t=2.425$, $df=9$	

+ -	S4E	Unpaired t-test	Results para 9	10	WT=6, HT=4	Fig legend	Error bars are mean +/- SEM	Fig legend	p=0.9069	Fig legend	t=0.1207, df=8	
+ -	S4F	Unpaired t-test	Results para 9	11	WT=6, HT=5	Fig legend	Error bars are mean +/- SEM	Fig legend	p=0.0248	Fig legend	t=2.464, df=9	
+ -	S4G	Unpaired t-test	Results para 9	14	WT=7, HT=7	Fig legend	Error bars are mean +/- SEM	Fig legend	p=0.0264	Fig legend	t=2.994, df=8	
+ -	S4H	Unpaired t-test	Results para 9	11	WT=6, HT=5	Fig legend	Error bars are mean +/- SEM	Fig legend	p=0.5476	Fig legend	t=0.6248, df=9	
+ -	S4I	Unpaired t-test	Results para 9	11	WT=6, HT=5	Fig legend	Error bars are mean +/- SEM	Fig legend	p=0.0581	Fig legend	t=2.17, df=9	
+ -	S4J	Unpaired t-test	Results para 9	10	WT=6, HT=4	Fig legend	Error bars are mean +/- SEM	Fig legend	p=0.1174	Fig legend	t=1.755, df=8	
+ -	S5A	RSAT de novo motif analysis	Results para 10	708	708 ChIP-seq peaks from WT=2	Methods	Predicted sites, logo motif bit scores	Fig	All relevant stats reported in table: YY1: e=4.2E-31, NRF1: e=8.5E-24, NFYB: e=1.3e-17	Fig	All relevant stats reported in table	Fig
+ -	S5D	Generalized linear regression model	Results para 13	44	WT=18, HT=26 littermates	Table S2	Mean +/- 1 SD	Table S4	Scn2b: FDR=3.9E-02 Cacna1e: FDR=1.2E-01 Cacna2d1: FDR=6.2E-02 Cacna1b: FDR=1.2E-01	Table S4	All relevant stats reported	Table S4
+ -	S5B	Generalized linear regression model	Results para 12	44, 37, 77	Gompers: WT=18, HT=26 littermates Katayama: 37 Durak: 77	Table S2	NA	NA	All relevant stats reported	Table S4	All relevant stats reported	Table S4
+ -	S5C	Generalized linear regression model	Results para 12	44, 37, 77	Gompers: WT=18, HT=26 littermates Katayama: 37 Durak: 77	Table S2	NA	NA	All relevant stats reported	Table S4	All relevant stats reported	Table S4
+ -	S6A	Student's t-test (type 3, 2-tailed)	Results para 15	18, 17	P0: WT=8, HT=10 P7: WT=7, HT=10	Fig legend	NA		P0: Tbr1: p=0.34 Ctip2: p=0.81	Fig legend	P0: df=4 Tbr1: t=0.75 Ctip2: t=0.46	
+ -	S6B	Student's t-test (type 3, 2-tailed)	Results para 15	18, 17	P0: WT=8, HT=10 P7: WT=7, HT=10	Fig legend	NA					
+ -	S6C	Student's t-test (type 3, 2-tailed)	Results para 15	18, 17	P0: WT=8, HT=10 P7: WT=7, HT=10	Fig legend	NA					
+ -	S6D	Student's t-test (type 3, 2-tailed)	Results para 15	18, 17	P0: WT=8, HT=10 P7: WT=7, HT=10	Fig legend	NA					
+ -	S6E	Student's t-test (type 3, 2-tailed)	Results para 15	18, 17	P0: WT=8, HT=10 P7: WT=7, HT=10	Fig legend	NA					
+ -	S6F	Student's t-test (type 3, 2-tailed)	Results para 15	18, 17	P0: WT=8, HT=10 P7: WT=7, HT=10	Fig legend	NA					
+ -	S6G	Student's t-test (type 3, 2-tailed)	Results para 15	18, 17	P0: WT=8, HT=10 P7: WT=7, HT=10	Fig legend	NA					
+ -	S6H	Student's t-test (type 3, 2-tailed)	Results para 15	18, 17	P0: WT=8, HT=10 P7: WT=7, HT=10	Fig legend	NA					

+ -	S6I	NA	Results para 15	18, 17	P0: WT=8, HT=10 P7: WT=7, HT=10	Fig legend	NA		P7: Tbr1: p=0.88 Ctip2: p=0.69 Brn2: p=0.32	Fig legend	P7: df=4 Tbr1: t=0.75 Ctip2: t=0.46 Brn2: 0.75	
+ -	S6J	NA	Results para 15	18, 17	P0: WT=8, HT=10 P7: WT=7, HT=10	Fig legend	NA					
+ -	S6K	NA	Results para 15	18, 17	P0: WT=8, HT=10 P7: WT=7, HT=10	Fig legend	NA					
+ -	S6L	NA	Results para 15	18, 17	P0: WT=8, HT=10 P7: WT=7, HT=10	Fig legend	NA					
+ -	S6M	NA	Results para 15	18, 17	P0: WT=8, HT=10 P7: WT=7, HT=10	Fig legend	NA					
+ -	S6N	NA	Results para 15	18, 17	P0: WT=8, HT=10 P7: WT=7, HT=10	Fig legend	NA					
+ -	S6O	NA	Results para 15	18, 17	P0: WT=8, HT=10 P7: WT=7, HT=10	Fig legend	NA					
+ -	S6P	NA	Results para 15	18, 17	P0: WT=8, HT=10 P7: WT=7, HT=10	Fig legend	NA					
+ -	S6Q	NA	Results para 15	18, 17	P0: WT=8, HT=10 P7: WT=7, HT=10	Fig legend	NA					
+ -	S6R	NA	Results para 15	18, 17	P0: WT=8, HT=10 P7: WT=7, HT=10	Fig legend	NA					
+ -	S7A	Permutation test: gene set compared for test and random sample (100k) set against DE genes	Results para 17	44	WT=18, HT=26 littermates	Table S2	Count (red line)	Table S3	Left: p=1.1e-03, Middle: 1.2e-10, Right: 1.2e-17	Fig	Relevant stats reported	Table S3
+ -	S7B	Welch's t-test, generalized linear regression	Results para 18	41	e12.5=7 e14.5=9 e17.5-WT=7 e17.5-HT=7 P0=11	Fig legend	Error bars are mean +/- SEM	Fig	e14.5-e17.5-HT: p=0.30 e17.5-HT-WT: p=0.62 Dev time: p=1.32E-05 R2=0.37	Fig legend	Dev time: e14.5-e17.5-HT: t=1.0847, df=13.9 e17.5-HT-WT: t=0.51739, df=10.666	Fig legend
+ -	S1D	NA										

► Representative figures

- Are any representative images shown (including Western blots and immunohistochemistry/staining) in the paper?

If so, what figure(s)?

Western blot data is presented in Figures 1E, 4E, and S1. IHC data is presented in Figures 6E, 7A-D, S6.

- For each representative image, is there a clear statement of how many times this experiment was successfully repeated and a discussion of any limitations in repeatability?

If so, where is this reported (section, paragraph #)?

Yes to all, and is reported in the above statistics reporting table as well as the following:

- Full western blot data and is displayed in Figure S1
- IHC data is described in figure legends (6E, 7A-D, S6)

► Statistics and general methods

1. Is there a justification of the sample size?

If so, how was it justified?

Where (section, paragraph #)?

Even if no sample size calculation was performed, authors should report why the sample size is adequate to measure their effect size.

Behavioral analysis sample size is justified in Paragraph 3, Statistics.

No justification of sample size is reported as power analysis is not standardized for RNA-seq. However, sample size per group and condition is equal to or greater than generally accepted standard of three biological replications per group. Our sample size is additionally sufficient for network analysis. This is reported in Para 2, Statistics.

No justification of sample size for other experiments, though biological replicate numbers are standard in the field and sufficient to capture significance and trends. This is reported in Para 1, Statistics.

2. Are statistical tests justified as appropriate for every figure?

Where (section, paragraph #)?

Behavioral analysis sample size is justified in Paragraph 3, Statistics.

We use standard statistical approaches with appropriate corrections for each experiment.

a. If there is a section summarizing the statistical methods in the methods, is the statistical test for each experiment clearly defined?

Behavioral analysis statistical tests are delineated within the text in Paragraph 3, Statistics.

For RNA-seq, yes, for each method described, in the relevant Methods sections.

All statistical methods reported in full in the text or supplement.

b. Do the data meet the assumptions of the specific statistical test you chose (e.g. normality for a parametric test)?

Where is this described (section, paragraph #)?

Behavioral analysis data meets the assumptions of the statistical tests chosen. Data passed distribution normality tests, was collected using continuous variables and thus analyzed via parametric analysis, in all assays. This is described in Para 3, Statistics.

Yes - QC performed to examine specific parameters and we used tests specifically designed for RNA-seq differential expression analysis. Additionally, we use non-parametric tests where necessary. This is described within the text in paragraph 1, subsection "RNA sequencing," of section "Methods."

c. Is there any estimate of variance within each group of data?

Is the variance similar between groups that are being statistically compared?

Where is this described (section, paragraph #)?

Behavioral analysis variances are similar within each group and between groups that are being statistically compared. This is described within the text in Paragraph 1 of "Behavioral Testing" in the "Methods".

For genomics, analysis methods are designed to be robust to sample variance. Further, we perform QC on individual samples to ensure robust comparisons. This is described within the text in paragraph 1 of Genomics in Methods.

For other analysis (e.g. qPCR and western blot), we used standard approaches (e.g. Student's t-test and ANOVA) in the field.

d. Are tests specified as one- or two-sided?

Always two-sided.

- e. Are there adjustments for multiple comparisons?
- Yes for behavior.
Yes for RNA-seq.
Yes for MRI.
3. To promote transparency, *Nature Neuroscience* has stopped allowing bar graphs to report statistics in the papers it publishes. If you have bar graphs in your paper, please make sure to switch them to dot-plots (with central and dispersion statistics displayed) or to box-and-whisker plots to show data distributions.
- All figures converted to show individual data points and summary/ variance measurements.
4. Are criteria for excluding data points reported?
Was this criterion established prior to data collection?
Where is this described (section, paragraph #)?
- We followed established laboratory protocol in which all data points that lie within 2 standard deviations of the mean are included in analysis. This is described within the text in Para 3 of Statistics.
- No data points excluded in RNA-seq after original quality filtering to remove samples with 3' coverage bias. This is described in the results and methods. For MISO analysis, one sample (e17.5 S159) was removed before pooling samples; this is reported in Para 1 of Miso Analysis in Methods.
- For qPCR, the highest and lowest values for both WT and Chd8+/del5 groups were removed to reduce variation. This was described in qRT-PCR in Methods; actual n's are listed in the figure legends.
- One of each sample from WT and HT in the Q-fraction analysis was removed; this is mention in Paragraph 1 of section "EdU labeling and immunofluorescent analysis" in "Methods".
5. Define the method of randomization used to assign subjects (or samples) to the experimental groups and to collect and process data.
If no randomization was used, state so.
Where does this appear (section, paragraph #)?
- Behavioral analysis was performed on mixed genotype home cages and blinded to experimenter and video scorer/processor. This is described within the text in paragraph 1 of "Nissl staining, EdU labeling, and immunofluorescent analysis" in Methods.
- For RNA-seq: samples were randomly collected across litters from male het x female wt and processed without knowing genotype. This is described in paragraph 4 of Statistics.
- Samples for western blot analysis were randomly collected from multiple litters. For all histology, samples were randomly selected for analysis, as described in Statistics, and additionally in methods.
6. Is a statement of the extent to which investigator knew the group allocation during the experiment and in assessing outcome included?
If no blinding was done, state so.
Where (section, paragraph #)?
- The investigator was blinded to behavioral experiments and analysis and to histology. This is described within the text in the first paragraph of subsections "Behavioral testing" and "Lamination Assay" in Methods.
- All experiments were performed blind to genotype ("Results" section, paragraph 1), unless denoted otherwise in Methods.
7. For experiments in live vertebrates, is a statement of compliance with ethical guidelines/regulations included?
Where (section, paragraph #)?
- A statement of compliance with ethical guidelines and regulations is included in both the methods and subsection "Behavioral testing" of Methods.

8. Is the species of the animals used reported?
Where (section, paragraph #)?
- The species of animal used in is given and described within the text in Paragraph 1 of section "Mice harboring heterozygous germline Chd8 mutation exhibit megalencephaly" in "Results".
9. Is the strain of the animals (including background strains of KO/transgenic animals used) reported?
Where (section, paragraph #)?
- Animal strain information is included in Paragraph 1 of section "Mice harboring heterozygous germline Chd8 mutation exhibit megalencephaly" in Results, and in Methods.
10. Is the sex of the animals/subjects used reported?
Where (section, paragraph #)?
- The sex of animals used in the behavioral analysis is described within the text in paragraph 1, section "Behavioral phenotyping of adult Chd8+/del5 mice " in Results, and additionally in Methods and Figure Legends.
- Full RNA-seq sample info given in Table S2.
Sex of animals used in western blots and histology was not described.
11. Is the age of the animals/subjects reported?
Where (section, paragraph #)?
- The age of animals used in the behavioral analysis is described within the text in paragraph 1 of "Behavioral Testing" in Methods.
- The age of animals used in RNA-seq is described within the text in paragraph 1 of section "Genomics" in "Experimental Procedures".
- The age of animals used in western blot is described within the figure legends and in text in the first paragraphs of "Generation of Chd8 mutant mice" and "Western blot analysis" of Methods.
12. For animals housed in a vivarium, is the light/dark cycle reported?
Where (section, paragraph #)?
- The environmental light conditions of the vivarium in which the animals used in the behavioral analysis is described within the text in paragraph 1 of "Behavioral Testing" in Methods.
13. For animals housed in a vivarium, is the housing group (i.e. number of animals per cage) reported?
Where (section, paragraph #)?
- The number animals per cage used in the behavioral analysis is described within the text in paragraph 1 of "Behavioral Testing" in Methods.
14. For behavioral experiments, is the time of day reported (e.g. light or dark cycle)?
Where (section, paragraph #)?
- The environmental light of the behavioral testing conditions in which the animals used in the behavioral analysis is described within the text in paragraph 1 of "Behavioral Testing" in Methods.
15. Is the previous history of the animals/subjects (e.g. prior drug administration, surgery, behavioral testing) reported?
Where (section, paragraph #)?
- Animals used in the behavioral analysis were not previously subjected to other assays or analysis. This is described within the text in paragraph 1 of "Behavioral Testing" in Methods.
- a. If multiple behavioral tests were conducted in the same group of animals, is this reported?
Where (section, paragraph #)?
- Animals used in the behavioral analysis were subjected to a set sequence of behavioral assays. This is described within the text in paragraph 1 of "Behavioral Testing" in Methods.
16. If any animals/subjects were excluded from analysis, is this reported?
Where (section, paragraph #)?
- No data points were excluded from behavioral analysis. This is described within the text in paragraph 3 of Statistics in Methods.

a. How were the criteria for exclusion defined?
Where is this described (section, paragraph #)?

N/A

b. Specify reasons for any discrepancy between the number of animals at the beginning and end of the study.
Where is this described (section, paragraph #)?

One animal died during behavioral testing. This happened during Three-Chambered Social approach, in the middle of the behavioral battery. This is described in paragraph 3 of Statistics in Methods.

► Reagents

1. Have antibodies been validated for use in the system under study (assay and species)?

Yes, except for Tbr2.

a. Is antibody catalog number given?
Where does this appear (section, paragraph #)?

Yes, in methods.

b. Where were the validation data reported (citation, supplementary information, Antibodypedia)?
Where does this appear (section, paragraph #)?

Antibodies used in previous studies are cited in the methods. For Tbr2, we cite the Abcam data sheet. The Tbr2 antibody exhibits similar histology staining patterns to other Tbr2 antibodies.

2. Cell line identity

a. Are any cell lines used in this paper listed in the database of commonly misidentified cell lines maintained by [ICLAC](#) and [NCBI Biosample](#)?
Where (section, paragraph #)?

NA

b. If yes, include in the Methods section a scientific justification of their use--indicate here in which section and paragraph the justification can be found.

NA

c. For each cell line, include in the Methods section a statement that specifies:
- the source of the cell lines
- have the cell lines been authenticated? If so, by which method?
- have the cell lines been tested for mycoplasma contamination?
Where (section, paragraph #)?

NA

► Data availability

Provide a Data availability statement in the Methods section under "Data availability", which should include, where applicable:

- Accession codes for deposited data
- Other unique identifiers (such as DOIs and hyperlinks for any other datasets)
- At a minimum, a statement confirming that all relevant data are available from the authors
- Formal citations of datasets that are assigned DOIs
- A statement regarding data available in the manuscript as source data
- A statement regarding data available with restrictions

See our [data availability and data citations policy page](#) for more information.

Data deposition in a public repository is mandatory for:

- Protein, DNA and RNA sequences
- Macromolecular structures
- Crystallographic data for small molecules
- Microarray data

Deposition is strongly recommended for many other datasets for which structured public repositories exist; more details on our data policy are available [here](#). We encourage the provision of other source data in supplementary information or in unstructured repositories such as [Figshare](#) and [Dryad](#).

We encourage publication of Data Descriptors (see [Scientific Data](#)) to maximize data reuse.

Where is the Data Availability statement provided (section, paragraph #)?

Data availability reported in methods with DOIs.

► Computer code/software

Any custom algorithm/software that is central to the methods must be supplied by the authors in a usable and readable form for readers at the time of publication. However, referees may ask for this information at any time during the review process.

1. Identify all custom software or scripts that were required to conduct the study and where in the procedures each was used.

Described in methods. All analysis software was previously published.

2. If computer code was used to generate results that are central to the paper's conclusions, include a statement in the Methods section under "**Code availability**" to indicate whether and how the code can be accessed. Include version information as necessary and any restrictions on availability.

Code availability:

All custom scripts and TrackHubs used for data processing and analysis will be available at the Nord Lab Git Repository (<https://github.com/NordNeurogenomicsLab/>).

► Human subjects

- | | |
|---|----|
| 1. Which IRB approved the protocol?
Where is this stated (section, paragraph #)? | NA |
| 2. Is demographic information on all subjects provided?
Where (section, paragraph #)? | NA |
| 3. Is the number of human subjects, their age and sex clearly defined?
Where (section, paragraph #)? | NA |
| 4. Are the inclusion and exclusion criteria (if any) clearly specified?
Where (section, paragraph #)? | NA |
| 5. How well were the groups matched?
Where is this information described (section, paragraph #)? | NA |
| 6. Is a statement included confirming that informed consent was obtained from all subjects?
Where (section, paragraph #)? | NA |
| 7. For publication of patient photos, is a statement included confirming that consent to publish was obtained?
Where (section, paragraph #)? | NA |

► fMRI studies

For papers reporting functional imaging (fMRI) results please ensure that these minimal reporting guidelines are met and that all this information is clearly provided in the methods:

- | | |
|--|----|
| 1. Were any subjects scanned but then rejected for the analysis after the data was collected? | NA |
| a. If yes, is the number rejected and reasons for rejection described?
Where (section, paragraph #)? | NA |
| 2. Is the number of blocks, trials or experimental units per session and/or subjects specified?
Where (section, paragraph #)? | NA |
| 3. Is the length of each trial and interval between trials specified? | NA |
| 4. Is a blocked, event-related, or mixed design being used? If applicable, please specify the block length or how the event-related or mixed design was optimized. | NA |

5. Is the task design clearly described?
Where (section, paragraph #)? NA
6. How was behavioral performance measured? NA
7. Is an ANOVA or factorial design being used? NA
8. For data acquisition, is a whole brain scan used?
If not, state area of acquisition. NA
- a. How was this region determined? NA
9. Is the field strength (in Tesla) of the MRI system stated? NA
- a. Is the pulse sequence type (gradient/spin echo, EPI/spiral) stated? NA
- b. Are the field-of-view, matrix size, slice thickness, and TE/TR/flip angle clearly stated? NA
10. Are the software and specific parameters (model/functions, smoothing kernel size if applicable, etc.) used for data processing and pre-processing clearly stated? NA
11. Is the coordinate space for the anatomical/functional imaging data clearly defined as subject/native space or standardized stereotaxic space, e.g., original Talairach, MNI305, ICBM152, etc? Where (section, paragraph #)? NA
12. If there was data normalization/standardization to a specific space template, are the type of transformation (linear vs. nonlinear) used and image types being transformed clearly described? Where (section, paragraph #)? NA
13. How were anatomical locations determined, e.g., via an automated labeling algorithm (AAL), standardized coordinate database (Talairach daemon), probabilistic atlases, etc.? NA
14. Were any additional regressors (behavioral covariates, motion etc) used? NA
15. Is the contrast construction clearly defined? NA
16. Is a mixed/random effects or fixed inference used? NA
- a. If fixed effects inference used, is this justified? NA
17. Were repeated measures used (multiple measurements per subject)? NA

- a. If so, are the method to account for within subject correlation and the assumptions made about variance clearly stated?
18. If the threshold used for inference and visualization in figures varies, is this clearly stated?
19. Are statistical inferences corrected for multiple comparisons?
- a. If not, is this labeled as uncorrected?
20. Are the results based on an ROI (region of interest) analysis?
- a. If so, is the rationale clearly described?
- b. How were the ROI's defined (functional vs anatomical localization)?
21. Is there correction for multiple comparisons within each voxel?
22. For cluster-wise significance, is the cluster-defining threshold and the corrected significance level defined?

► Additional comments

Additional Comments

Efforts have been made to report specific methods in the manuscript or in the methods section. We will make our raw data, processed data, and analysis codes available via our GitHub site.